J. Fluid Mech. (2010), *vol.* 655, *pp.* 472–503.
doi:10.1017/S002211201000100X

A fibre-reinforced fluid model of anisotropic plant cell growth

R. J. DYSON[1]† AND O. E. JENSEN[1,2]

[1]Centre for Plant Integrative Biology, School of Biosciences, University of Nottingham, Sutton Bonington LE12 5RD, UK

[2]School of Mathematical Sciences, University of Nottingham, University Park, Nottingham NG7 2RD, UK

(Received 13 July 2009; revised 16 February 2010; accepted 22 February 2010)

Many growing plant cells undergo rapid axial elongation with negligible radial expansion. Growth is driven by high internal turgor pressure causing viscous stretching of the cell wall, with embedded cellulose microfibrils providing the wall with strongly anisotropic properties. We present a theoretical model of a growing cell, representing the primary cell wall as a thin axisymmetric fibre-reinforced viscous sheet supported between rigid end plates. Asymptotic reduction of the governing equations, under simple sets of assumptions about the fibre and wall properties, yields variants of the traditional Lockhart equation, which relates the axial cell growth rate to the internal pressure. The model provides insights into the geometric and biomechanical parameters underlying bulk quantities such as wall extensibility, and shows how either dynamical changes in wall material properties or passive fibre reorientation may suppress cell elongation.

1. Introduction

Cell growth is a fundamental feature of plant biology (Taiz & Zeiger 2002), with differential growth underlying essential processes such as gravitropism and morphogenesis. Broadly speaking, growing plant cells fall into two categories: cells which exhibit tip growth (such as root hairs or pollen tubes, where wall expansion is localized to the tip of the cell; see the review by Geitmann 2006); and those which exhibit diffuse growth (where growth occurs over the entire cell length). The primary root of the model species *Arabidopsis thaliana* (Scheres, Benfey & Dolan 2002) provides a canonical example of diffuse growth. The portion of the root in which the majority of growth occurs can be divided into two zones: the meristem, where cells are created, divide and differentiate, and the elongation zone, where cells undergo rapid anisotropic expansion, increasing in length by 30-fold at essentially constant radius (see figure 1). Cell growth within the elongation zone is the main driver of expansion within the root, pushing its tip forward into the surrounding environment. Relative to the advancing tip, it takes a cell around 100 h to move 350 μm through the meristem to the elongation zone, but only 6 h to traverse the 1000 μm elongation zone. The internodal cells of aquatic algae such as *Chara* (Proseus, Zhu & Boyer 2000) or *Nitella* (Green 1968) also display diffuse expansion. These large cells combine into branching structures to form multicellular algae, but will also

† Email address for correspondence: rosemary.dyson@cpib.ac.uk

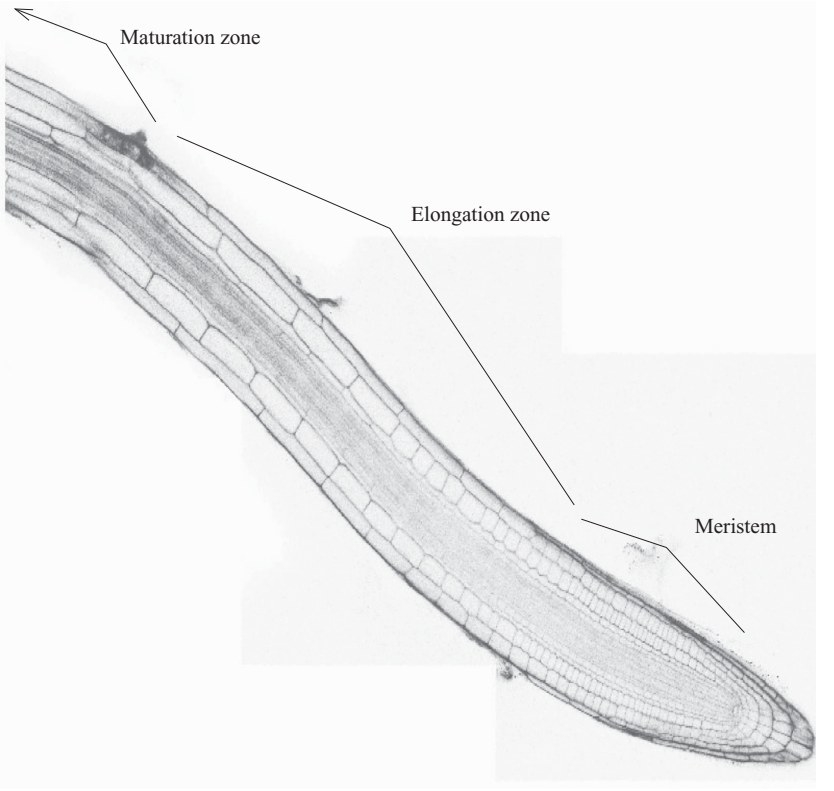

FIGURE 1. The growing root of *Arabidopsis thaliana* showing the meristem and elongation zone and illustrating the significant anisotropic expansion of the cells. Image courtesy of Susana Ubeda-Tomás, Centre for Plant Integrative Biology, University of Nottingham.

expand when isolated from other cells, making them another popular experimental system to examine diffuse expansion (Probine & Preston 1961, 1962; Probine 1963; Proseus, Ortega & Boyer 1999).

Plant cells are pressurized structures surrounded by a tough cell wall, a complex material capable of maintaining remarkably high turgor pressures of up to several megapascals (tens of bar) (Tomos 2000) while allowing significant cell expansion. Cells are tightly adhered to their neighbours, requiring the growth of individual cells in a whole organ to be highly regulated (Lindenmayer *et al.* 1996). The primary wall of a root cell consists of oriented cellulose microfibrils (CMF), cross-linked through a network of hemicellulose tethers, embedded within a pectin ground matrix. Hoop-like orientation of CMF in cylindrical cells creates strong anisotropy in the cell wall properties, promoting growth axially and restricting growth radially (see Somerville *et al.* 2004 for a review).

Cells in the root expansion zone grow through a process of stress relaxation: the internal turgor pressure, which is regulated on the order of seconds by the cell's osmotic potential (Zhu & Steudle 1991) and is therefore essentially constant on the time scale of growth, creates a tension within the walls which causes irreversible viscous deformation (creep) of the wall. The degree of creep is controlled by the cell wall mechanical properties, which in turn are altered by enzyme activity, e.g. by expansins (McQueen-Mason & Cosgrove 1995) that disconnect cross-linkers from

CMF, xyloglucan endotransglycosylases (van Sandt *et al.* 2007) that cleave cross-linkers and pectin methyl esterases (Jarvis 1984; Derbyshire, McCann & Roberts 2007*b*) that soften the ground matrix (see Cosgrove 2005 for a recent review). Enzyme activity is regulated by changes in hormone concentrations (Dolan & Davies 2004). To retain the integrity of the growing wall, new material is continually deposited on the inner face (Richmond, Metraux & Taiz 1980). A summary of recent experimental work on the mechanics of growth is given in Schopfer (2006), while reviews of the regulation of plant cell expansion are given in Taiz (1984), Baskin (2005) and Thompson (2005).

Many theoretical models of diffuse plant cell growth are built on the widely used model of Lockhart (1965), which treats the cell as a linear viscoplastic compartment under osmotic control. The Lockhart model consists of coupled equations for water uptake, controlled by the cell's osmotic potential, and cell growth, which is driven by this water uptake. When water availability is not rate limiting, the osmotic potential quickly adjusts to maintain a constant turgor pressure within the growing cell and so only the cell growth equation need be considered. For a hollow circular cylindrical cell of radius R^* and wall thickness h^*, the internal pressure P^* acting on the cell end plates induces an axial tension $T^* = P^*R^*/2h^*$ within the walls. This tension causes irreversible growth of the cell wall via a Bingham-type law

$$\frac{1}{l^*}\frac{\mathrm{d}l^*}{\mathrm{d}t^*} = \Phi^*(T^* - Y^*) \tag{1.1}$$

$$= \Phi^*\left(\frac{P^*R^*}{2h^*} - Y^*\right), \tag{1.2}$$

when $T^* > Y^*$, where $l^*(t^*)$ is the length of the cell at time t^*, Φ^* is the extensibility (dimensionally equivalent to an inverse viscosity) and Y^* is a yield stress. Within the literature, the extensibility and yield are often scaled to remove the geometric factors, leading to

$$\frac{1}{l^*}\frac{\mathrm{d}l^*}{\mathrm{d}t^*} = \overline{\Phi}^*(P^* - \overline{Y}^*) \text{ for } P^* > \overline{Y}^*. \tag{1.3}$$

This model has been extended to include elastic effects when $T^* < Y^*$ (Ortega 1985). Equation (1.2) is also often used to model the growth of cell walls in multicellular systems (Chavarria-Krauser, Jager & Schurr 2005). Some work has been undertaken to express Φ^* and Y^* in terms of the molecular components of the cell wall (Passioura & Fry 1992; Veytsman & Cosgrove 1998), in particular considering the bonds between the CMF and hemicellulose, although these models neglect the effect of the pectin matrix within which the fibres are embedded.

The aim of the present paper is to develop a theoretical model for a growing plant cell that is firmly based on mechanical principles, that can in principle be integrated with detailed models of enzyme and hormone action and that underpins Lockhart's macroscopic cell-growth equation (1.2). The cell wall material will be approximated as a thin sheet of viscous fluid, ignoring elastic effects that might operate over shorter time scales and assuming the wall is permanently yielded, but accounting carefully for the anisotropic stresses arising from the reinforcement of the wall by CMF. We wish to gain insight into the fluid-mechanical factors contributing to the wall's effective extensibility, and to understand the conditions under which simple linear relationship (1.2) may or may not hold.

There is considerable debate within the plant science community over the arrangement of CMF in the cell wall. It is well established that the orientation

of the CMF determines the mechanical anisotropy of the wall (Suslov & Verbelen 2006), however how this orientation is controlled is less clear. The orientation of newly deposited CMF may be determined by that of cortical microtubules, however some recent evidence contradicts this view (Baskin 2001; Lloyd & Chan 2004; Smith & Oppenheimer 2005). In turn, the microtubule angle can be affected by global cell properties, for example aligning with the principle stress directions (Hamant *et al.* 2008). Similarly there is evidence both supporting and refuting the idea that CMF are passively reorientated as the wall stretches (Kerstens & Verbelen 2003; Marga *et al.* 2005). The traditional multinet theory that CMF are laid down transversely on the inner face of the cell wall, and passively reorientate, becoming more longitudinal towards the outer face of the wall (Green 1960; Gertel & Green 1977) is supported by recent experimental evidence (Anderson *et al.* 2010). In the absence of a definitive view on this issue, we will make the simple assumption that the fibres passively reorientate as the wall elongates. Likewise, there is debate about the degree of cell wall deposition during growth (Derbyshire *et al.* 2007*a*); for simplicity we will assume the wall to have constant thickness during growth, and that new fibres are deposited at the angle of the current wall configuration, assumptions that yield a useful leading-order approximation. We also briefly treat the case in which fibres are laid down at a fixed orientation at the inner wall, so that the fibre orientation must be averaged across the cell wall in order to describe the wall's effective mechanical properties.

Bruce (2003) provides a comprehensive review of mathematical modelling applied to the mechanical behaviour of plant systems at the cellular to tissue scale. Most previous plant wall models address the short-term elastic properties of the material, in contrast to the longer-term viscous response of individual growing cells; however it should be recognized that slow differential growth can lead to residual elastic stresses in multicellular tissues (Goriely *et al.* 2008). The elastic models increase in complexity from linear isotropic (Pitt & Davis 1984) and transversely isotropic (Cowdrey & Preston 1966; Sellen 1983) to nonlinear models that either neglect wall anisotropy (Davies, Hiller & Bruce 1998) or incorporate it through an additive decomposition of the strain energy with a matrix term and a fibre term (Hettiaratchi & O'Callaghan 1978; Chaplain 1993). The first three models mentioned do not deal with growth but are concerned with inferring elastic properties from experimental data (Cowdrey & Preston 1966; Davies *et al.* 1998) or modelling the tissue-scale composite behaviour of multiple pressurized cells (Pitt & Davis 1984). Sellen's (1983) model of a transversely isotropic elastic cylinder deformed by an internal pressure could give a model for growth if the material properties were to vary in time, leading to time-dependent expansion. In contrast, Hettiaratchi & O'Callaghan (1978) and Chaplain (1993) both calculate steady-state pressure–volume curves, assuming (in line with the prevailing theory at the time) that cell growth is achieved through increases in turgor pressure, a theory now discredited. Among models which treat the plant cell wall as a viscous material is the anisotropic–viscoplastic model for tip growth derived by Dumais *et al.* (2006), which includes the effects of the mechanical anisotropy of the wall material as well as the observed yield.

The Dumais *et al.* (2006) model for tip growth has similarities in form with our fluid-mechanical model of diffuse growth, however the wall in each case has contrasting properties and hence the constitutive laws are significantly different. In both cases transverse isotropy is displayed, however the orientation of the preferred material direction differs. At the dome of tip-growing cells, fibres lie randomly in the plane of the wall, so that the in-plane material properties are different from those normal to the wall. In contrast, in our model of a diffusely growing cell we

assume fibres are orientated in one preferred direction within the plane of the wall, so that material properties in the fibre direction differ from those in the orthogonal plane. Accordingly we treat the cell wall as a fibre-reinforced composite, following approaches for nematic liquid crystals (Ben Amar & Cummings 2001), textile fibre composites (Lee & Ockendon 2005) and the extensional flow of collagen gels (Green & Friedman 2008). We use a linear constitutive relation for a transversely isotropic material with a single preferred direction (representing the fibre direction), exploiting formulations identified by Ericksen (1960) and Spencer (1972); given the limited mechanical and structural data for the primary plant cell wall in the *Arabidopsis* root, we choose here not to implement the full nonlinear approach that has been developed for viscoelastic and viscoplastic fibre-reinforced materials by Holzapfel, Gasser & Ogden (2000) and others in other biomechanical applications. While Green & Friedman (2008) considered a thin planar fluid layer, we model the plant cell as an axisymmetric structure with a curved free film between rigid end plates, extending the framework derived by van de Fliert, Howell & Ockendon (1995) (referred to hereafter as VHO) for the pressure-driven flow of a thin-walled fluid sheet in the context of glass blowing. Our model therefore provides a generalization of the traditional Trouton description of extensional flows to account for an evolving microstructure. In § 2 we state the governing equations for the system and explain how they can be systematically simplified by asymptotic analysis. We then illustrate solutions in three special cases in § 3, each of which leads to an appropriate modification of (1.2). Results are described in § 4 and their implications discussed in § 5.

2. Governing equations

We assume cell growth is governed by creep in the cell wall induced by the turgor pressure. A single cell is approximated as an axisymmetric structure, formed from a sheet of viscous incompressible fluid (representing the cell wall) supported between rigid end plates and subject to a uniform internal pressure $P^*(t^*)$ at time t^*. The effects of neighbouring cells are represented by external longitudinal and radial compressive forces, Q^* and P^*_{ext} respectively, and an external torque, Σ^*, applied to the top end of the cell; the bottom end is assumed fixed (figure 2). We measure all pressures relative to the external radial compressive force, and so take $P^*_{ext} = 0$. Representing the cell wall as a viscous fluid assumes that it is permanently yielded and will exhibit irreversible deformation. We assume that the centreline of the cell remains straight as it elongates.

The equations of mass and momentum conservation in the cell wall (neglecting the effects of inertia, surface tension and gravity) are

$$\nabla^* \cdot \boldsymbol{U}^* = F^*(\boldsymbol{x}^*, t^*), \qquad \nabla^* \cdot \boldsymbol{\sigma}^* = 0, \tag{2.1}$$

where $\boldsymbol{U}^*(\boldsymbol{x}^*, t^*)$ is the fluid velocity relative to a fixed frame of reference with origin in the centre of the base plate (coordinate $\boldsymbol{x}^*$), $\boldsymbol{\sigma}^*(\boldsymbol{x}^*, t^*)$ is the stress tensor and $F^*(\boldsymbol{x}^*, t^*)$ is a prescribed source term which represents the deposition of new material onto the cell wall.

The components of the stress tensor must be defined using an appropriate constitutive relation. We consider the reinforcement of the plant cell wall by CMF to be due to a single family of extensible fibres with director field $\boldsymbol{a}(\boldsymbol{x}^*, t^*)$, such that $|\boldsymbol{a}| = 1$. Although the fibres will not all be perfectly aligned, we assume a tight distribution about the mean direction $\boldsymbol{a}$ and thus do not track the distribution

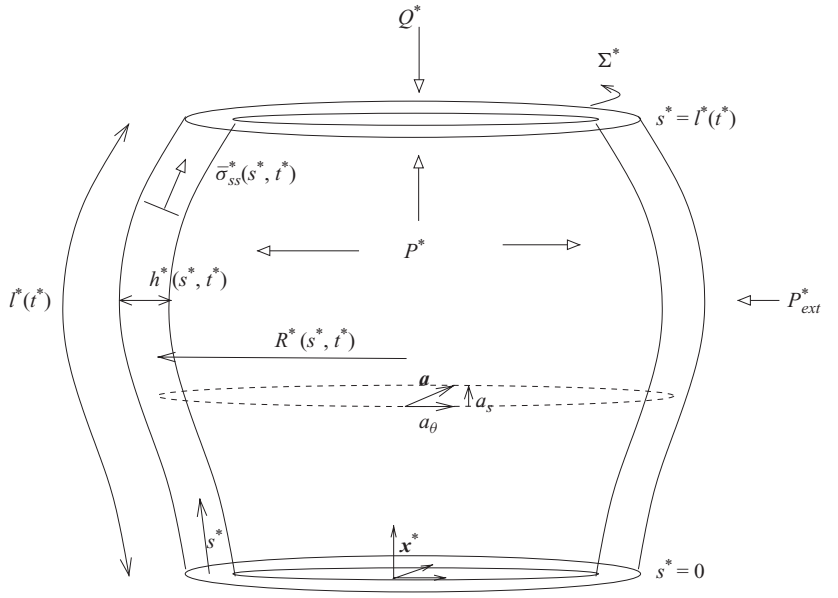

FIGURE 2. A cell represented by an axisymmetric fluid sheet with rigid end plates subject to an internal pressure. The cell walls consist of a viscous fluid containing oriented fibres.

explicitly. The director field satisfies the evolution equation

$$\frac{\partial \boldsymbol{a}}{\partial t^*} + \left(\boldsymbol{U}^* \cdot \nabla^*\right) \boldsymbol{a} + \zeta^* \boldsymbol{a} = \left(\boldsymbol{a} \cdot \nabla^*\right) \boldsymbol{U}^*, \tag{2.2}$$

so that the fibres are convected, stretched and reoriented by the flow, preserving unit length. Here, $\zeta^* = \boldsymbol{a} \cdot \mathbf{e}^* \cdot \boldsymbol{a}$, where $\mathbf{e}^* = (\nabla^* \boldsymbol{U}^* + \nabla^* \boldsymbol{U}^{*\mathrm{T}})/2$ is the strain rate, gives the strain rate in the fibre direction. A derivation of (2.2) is given in Green & Friedman (2008); this is a special case of a result derived in Ericksen (1960) and generalizes Jeffery's treatment of the motion of long ellipsoidal particles (Jeffery 1922), which align asymptotically in the direction of the principal rate of strain.

The fibre density, $\rho^*(\boldsymbol{x}^*, t^*)$, evolves according to

$$\frac{\partial \rho^*}{\partial t^*} + \nabla^* \cdot \left(\rho^* \boldsymbol{U}^*\right) = G^*(\boldsymbol{x}^*, t^*), \tag{2.3}$$

where $G^*(\boldsymbol{x}^*, t^*)$ is a prescribed source term representing deposition of new material.

The fibres induce transverse isotropy within the fluid aligned with the director field. We adopt a phenomenological constitutive relation that satisfies material frame indifference, neglects fibre inertia and is linear in the strain rate, taking a stress tensor of the form (Ericksen 1960; Hand 1962)

$$\sigma^*_{ij} = -p^* \delta_{ij} + 2\mu^*_0 e^*_{ij} + \mu^*_1 a_i a_j + \mu^*_2 a_i a_j a_k a_l e^*_{kl} + 2\mu^*_3 \left(a_i a_l e^*_{jl} + a_j a_m e^*_{mi}\right), \tag{2.4}$$

where δ_{ij} is the Kronecker delta. Here, p^* is the fluid pressure and the coefficients μ^*_0, μ^*_1, μ^*_2, μ^*_3 are parameters that depend on the local fibre density and may be functions of both time and space (as the cell exerts active control over growth via enzymatic and biochemical modification of the wall's properties). μ^*_0, μ^*_2 and μ^*_3 can be interpreted as viscosities in the following sense. For two-dimensional deformations in the plane of the fibres, the extensional viscosity parallel to the fibre direction is $\mu^*_\parallel \equiv \mu^*_0 + (\mu^*_2 + 4\mu^*_3)/2$, while that orthogonal to the fibre direction is $\mu^*_\perp \equiv \mu^*_0$; the

shear viscosity is $\mu_s^* \equiv \mu_0^* + \mu_3^*$. We therefore describe μ_0^* as the isotropic component of the matrix viscosity (modified by the presence of the fibres); μ_2^* contributes to $\mu_\parallel^*$ while μ_3^* distinguishes $\mu_\perp^*$ from μ_s^*. μ_1^* can be considered as a tension in the fibre direction. In § 3.3 we will follow Spencer (1972) and consider the limit of zero extensibility in the fibre direction ($\mu_2^* \to \infty$, $a_k a_l e_{kl}^* \to 0$ with their product remaining finite, treating the net tension $\mu_1^* + \zeta\mu_2^*$ as a Lagrange multiplier to enforce the kinematic constraint).

Constitutive relations of the form (2.4) emerge naturally in statistically homogeneous suspensions of dilute rigid rods; Batchelor (1970) showed how the stresslet generated due to an ellipsoid (determined originally by Jeffery 1922) can be used to relate the μ_i^* to the viscosity $\bar{\mu}$ of the suspending fluid (for details see Lipscomb *et al.* 1988). However the dilute limit requires individual rods to be very widely spaced; for the more realistic semi-dilute limit, in which the rod spacing is intermediate between rod radius and rod length, Batchelor (1971) showed how, in extensional flow of aligned rods, $\mu_2^* \propto \bar{\mu}\Psi r^2$ (modulo a logarithmic factor), where Ψ ($\ll 1$) is the volume fraction and r ($\gg 1$) the rod aspect ratio. This demonstrates how even small densities of sufficiently long CMF can make $\mu_\parallel^*$ substantially larger than $\bar{\mu}$.

The curved surfaces of the viscous sheet are assumed to be free of shear stress and subject to a transmural pressure difference and kinematic conditions. We prescribe zero velocity at the base of the cell, while the velocity at the top of the cell in conjunction with a force balance form the free-boundary problem for the *a priori* unknown growing length $l^*(t^*)$ of the cell. We also prescribe the initial size of the cell, the director field and the density of the fibres.

2.1. *Geometric simplification*

Following VHO, we exploit the slender geometry of the fluid sheet to derive a simplified system of governing equations. We employ a mixed moving coordinate system which is fixed within the fluid sheet, where s^*, the axial arclength along the centre-surface of the wall (measured from the base plate, see figure 2), and n^*, the distance from the centre-surface in the inward normal direction, are body-fitted coordinates while θ, the polar angle, is fixed in space. These coordinates have respective unit base vectors $\boldsymbol{e}_s$, $\boldsymbol{e}_\theta$, $\boldsymbol{e}_n$. We assume the cell to be axisymmetric, so we may neglect derivatives with respect to θ; however, the presence of the fibres allows for non-zero azimuthal velocity. We take $R^*(s^*, t^*)$ to be the radius of the centre-surface and $h^*(s^*, t^*)$ the thickness of the wall. In the reference frame of the base plate, the centre-surface of the sheet moves with velocity $\boldsymbol{v}^*(s^*, t^*) \equiv v_s^*\boldsymbol{e}_s + v_\theta^*\boldsymbol{e}_\theta + v_n^*\boldsymbol{e}_n$, with components which satisfy the kinematic constraints (see Appendix A)

$$0 = \frac{\partial v_s^*}{\partial s^*} - \kappa_s^* v_n^*, \tag{2.5a}$$

$$\frac{\partial R^*}{\partial t^*} = v_s^* \frac{\partial R^*}{\partial s^*} - R^* \kappa_\theta^* v_n^*, \tag{2.5b}$$

$$v_\theta^* \frac{\partial R^*}{\partial s^*} = R^* \frac{\partial v_\theta^*}{\partial s^*}, \tag{2.5c}$$

where the azimuthal and axial curvatures of the centre-surface are given by

$$\kappa_\theta^* = \frac{\Delta}{R^*}, \qquad \kappa_s^* = -\frac{1}{\Delta}\frac{\partial^2 R^*}{\partial s^{*2}}, \tag{2.6}$$

where

$$\Delta = \left(1 - \left(\frac{\partial R^*}{\partial s^*}\right)^2\right)^{1/2}. \tag{2.7}$$

We may therefore express the governing equations in terms of the fluid velocity relative to the moving centre-surface, that is $\boldsymbol{u}^* = \boldsymbol{U}^* - \boldsymbol{v}^*$, where $\boldsymbol{u}^*(s^*, t^*) \equiv u_s^* \boldsymbol{e}_s + u_\theta^* \boldsymbol{e}_\theta + u_n^* \boldsymbol{e}_n$. (Note that $\boldsymbol{v}^*$ is not a velocity of material elements, but arises from our geometric parametrization.)

We non-dimensionalize and rescale the system using

$$\left.\begin{aligned}
&\{n^*, h^*\} = \epsilon R_0 \{n, h\},\ t^* = \frac{\epsilon M_0}{P_0} t,\ \{\kappa_s^*, \kappa_\theta^*\} = \frac{\{\kappa_s, \kappa_\theta\}}{R_0},\ \{R^*, s^*, l^*\} = R_0\{R, s, l\},\\
&\rho^* = \rho_0 \rho,\ \{P^*, Q^*\} = P_0\{P, Q\},\ \zeta^* = \frac{P_0}{\epsilon M_0}\zeta,\ \{\mu_0^*, \mu_2^*, \mu_3^*\} = M_0\{\mu_0, \mu_2, \mu_3\},\\
&\mu_1^* = \frac{P_0}{\epsilon}\mu_1,\ G^* = \frac{\rho_0 P_0}{\epsilon M_0} G,\ F^* = \frac{P_0 R_0^2}{M_0} F,\ \{\boldsymbol{u}^*, \boldsymbol{v}^*, \boldsymbol{U}^*\} = \frac{R_0 P_0}{\epsilon M_0}\{\boldsymbol{u}, \boldsymbol{v}, \boldsymbol{U}\},\\
&\mathbf{e}^* = \frac{P_0}{\epsilon M_0}\mathbf{e},\ \{p^*, \boldsymbol{\sigma}^*\} = \frac{P_0}{\epsilon}\{p, \boldsymbol{\sigma}\},\ \Sigma^* = R_0 P_0 \Sigma,
\end{aligned}\right\} \tag{2.8}$$

where R_0 is the initial radius of the cell, $h_0 \equiv \epsilon R_0$ is the initial thickness of the wall (where the aspect ratio $\epsilon \ll 1$), M_0 is the initial matrix viscosity, ρ_0 is the initial fibre density and P_0 is the initial turgor pressure (all assumed uniform). Equations (2.5) and (2.6) become

$$0 = \frac{\partial v_s}{\partial s} - \kappa_s v_n, \tag{2.9a}$$

$$\frac{\partial R}{\partial t} = v_s \frac{\partial R}{\partial s} - R\kappa_\theta v_n, \tag{2.9b}$$

$$v_\theta \frac{\partial R}{\partial s} = R\frac{\partial v_\theta}{\partial s}, \tag{2.9c}$$

$$\kappa_\theta = \frac{\Delta}{R}, \qquad \kappa_s = -\frac{1}{\Delta}\frac{\partial^2 R}{\partial s^2}, \tag{2.10}$$

where $\Delta = (1 - (\partial R/\partial s)^2)^{1/2}$.

2.2. *Asymptotic simplification*

The system may be simplified by performing a formal asymptotic expansion of (2.1) in small ϵ. VHO found, to leading order from (2.1), $\boldsymbol{U} \cdot \boldsymbol{e}_n = v_n$, i.e. $u_n = 0$ and u_s, u_θ to be independent of n, leaving the system

$$\frac{\partial}{\partial t}(Rh) + \frac{\partial}{\partial s}(u_s Rh) = F(s, t), \tag{2.11}$$

$$\kappa_s \bar{\sigma}_{ss} + \kappa_\theta \bar{\sigma}_{\theta\theta} = P, \tag{2.12a}$$

$$\frac{\partial}{\partial s}(R^2 \kappa_\theta \bar{\sigma}_{ss}) = PR\frac{\partial R}{\partial s}, \tag{2.12b}$$

$$\frac{\partial}{\partial s}(R^2 \bar{\sigma}_{s\theta}) = 0, \tag{2.12c}$$

where $\bar{\sigma}_{ss}$, $\bar{\sigma}_{s\theta}$, $\bar{\sigma}_{\theta\theta}$ give the stress components integrated over the thickness of the sheet; $\bar{\sigma}_{ss}$ is the longitudinal tension within the sheet, $\bar{\sigma}_{\theta\theta}$ is the azimuthal tension and $\bar{\sigma}_{s\theta}$ is the tension caused by shear stresses. Here (2.11) represents conservation of mass, while (2.12*a–c*) give conservation of momentum normal, longitudinal and

azimuthal to the fluid sheet respectively. In general, the transmural pressure difference will remain constant throughout the motion, but we retain P in (2.12*a*,*b*) to allow for temporal variation of this parameter.

This system of equations was derived by VHO for a Newtonian fluid, but it can be adapted for any type of viscous fluid by modifying the stress tensor. We must perform an expansion similar to that in VHO to find the integrated stress tensors and the appropriately simplified evolution equations for the fibre director field and fibre density.

We assume that the fibres lie entirely in the plane of the fluid sheet, that is $\boldsymbol{a} = a_\theta \boldsymbol{e}_\theta + a_s \boldsymbol{e}_s$ as shown in figure 2. With the exception of Appendix D, we also assume for simplicity that the fibre orientation does not vary through the wall (fibres at the inner wall being laid down in the same local configuration as those in the wall). The axisymmetric fibre director field may therefore be expressed in terms of a single angle ϕ to the horizontal such that $\boldsymbol{a} = \cos\phi\, \boldsymbol{e}_\theta + \sin\phi\, \boldsymbol{e}_s$. However, we continue to use the notation a_s and a_θ for brevity where appropriate.

We first consider the evolution equation (2.2) for the fibre director field. We perform a similar asymptotic expansion (details are given in Appendix B.2) and, taking suitable linear combinations of the components of the resulting equations, find the evolution equation for the director angle ϕ to be

$$\frac{\partial \phi}{\partial t} + (u_s + v_s)\frac{\partial \phi}{\partial s} = \cos\phi \sin\phi \left(\frac{\partial u_s}{\partial s} - \frac{1}{R}\frac{\mathrm{D}R}{\mathrm{D}t} \right) - \sin^2\phi \left(\frac{\partial u_\theta}{\partial s} - \frac{u_\theta}{R}\frac{\partial R}{\partial s} \right), \quad (2.13)$$

and the strain rate in the fibre direction to be

$$\zeta = \frac{\cos^2\phi}{R}\frac{\mathrm{D}R}{\mathrm{D}t} + \cos\phi \sin\phi \left(\frac{\partial u_\theta}{\partial s} - \frac{u_\theta}{R}\frac{\partial R}{\partial s} \right) + \sin^2\phi \frac{\partial u_s}{\partial s}, \quad (2.14)$$

where $\mathrm{D}R/\mathrm{D}t = \partial R/\partial t + u_s \partial R/\partial s$ is the convective derivative moving with the centre-surface.

Expanding the fibre-density evolution equation (2.3) similarly (see Appendix B.3) we find

$$\frac{\partial \rho}{\partial t} + (u_s + v_s)\frac{\partial \rho}{\partial s} + \rho \left(\frac{1}{R}\frac{\mathrm{D}R}{\mathrm{D}t} + \frac{\partial u_s}{\partial s} \right) = G(s,t). \quad (2.15)$$

We now consider the stress components (2.4). Due to linearity we may consider each term within the stress tensor separately. The leading-order pressure term can be expressed in terms of u_s and R using only the expression for σ_{nn}. As $\boldsymbol{a}\cdot\boldsymbol{e}_n = 0$, this pressure is not modified from the Newtonian case (VHO) and we do not need to recalculate it; the pressure and matrix viscosity terms are

$$p = -2\mu_0 \frac{\partial u_s}{\partial s} - \frac{2\mu_0}{R}\frac{\mathrm{D}R}{\mathrm{D}t}. \quad (2.16)$$

Further details of the calculation are given in Appendix B.1.

We find the leading-order strain-rate components to be

$$e_{ss} = \frac{\partial u_s}{\partial s}, \quad (2.17a)$$

$$e_{s\theta} = \frac{1}{2}\left(\frac{\partial u_\theta}{\partial s} - \frac{u_\theta}{R}\frac{\partial R}{\partial s} \right), \quad (2.17b)$$

$$e_{\theta\theta} = \frac{1}{R}\frac{\mathrm{D}R}{\mathrm{D}t}. \quad (2.17c)$$

We retain an additional term in $e_{s\theta}$ which is missing in VHO (see Howell 1998). Given (2.14) and (2.17), it is straightforward to write down the integrated axial, azimuthal and shear tensions as

$$\bar{\sigma}_{ss} = \frac{2h}{R}\mu_0\left(2R\frac{\partial u_s}{\partial s} + \frac{\mathrm{D}R}{\mathrm{D}t}\right) + h\mu_1 a_s^2 + h\mu_2 a_s^2\zeta + 4h\mu_3\left(a_s^2\frac{\partial u_s}{\partial s} + \frac{a_s a_\theta}{2}\left(\frac{\partial u_\theta}{\partial s} - \frac{u_\theta}{R}\frac{\partial R}{\partial s}\right)\right), \tag{2.18a}$$

$$\bar{\sigma}_{s\theta} = h\mu_0\left(\frac{\partial u_\theta}{\partial s} - \frac{u_\theta}{R}\frac{\partial R}{\partial s}\right) + h\mu_1 a_s a_\theta + h\mu_2 a_s a_\theta\zeta + 2h\mu_3\left(\frac{1}{2}\left(\frac{\partial u_\theta}{\partial s} - \frac{u_\theta}{R}\frac{\partial R}{\partial s}\right) + \frac{a_s a_\theta}{R}\left(\frac{\mathrm{D}R}{\mathrm{D}t} + R\frac{\partial u_s}{\partial s}\right)\right), \tag{2.18b}$$

$$\bar{\sigma}_{\theta\theta} = \frac{2h}{R}\mu_0\left(R\frac{\partial u_s}{\partial s} + 2\frac{\mathrm{D}R}{\mathrm{D}t}\right) + h\mu_1 a_\theta^2 + h\mu_2 a_\theta^2\zeta + 4h\mu_3\left(\frac{a_\theta^2}{R}\frac{\mathrm{D}R}{\mathrm{D}t} + \frac{a_s a_\theta}{2}\left(\frac{\partial u_\theta}{\partial s} - \frac{u_\theta}{R}\frac{\partial R}{\partial s}\right)\right), \tag{2.18c}$$

retaining dimensionless viscosities to allow for their spatial and temporal variation.

2.3. *Boundary and initial conditions*

We prescribe the initial configuration via

$$h(s,0) = 1,\ \ R(s,0) = 1,\ \ \phi(s,0) = \phi_0,\ \ \rho(s,0) = 1,\ \ l(0) = l_0, \tag{2.19}$$

so the dimensional initial cell length is $l_0^* \equiv R_0 l_0$. The fluid sheet is fixed to the base of the cell, i.e.

$$u_s(0,t) = 0, \quad u_\theta(0,t) = 0, \quad v_s(0,t) = 0, \quad v_\theta(0,t) = 0, \quad R(0,t) = 1, \tag{2.20}$$

with conditions

$$\phi(0,t) = \phi_0,\ \ \rho(0,t) = 1,\ \ h(0,t) = 1. \tag{2.21}$$

At the other end of the cell, $s = l$, we prescribe the radius of the centre-surface

$$R(l,t) = 1, \tag{2.22}$$

and take

$$\bar{\sigma}_{s\theta}(l(t),t) = \Sigma(t); \tag{2.23}$$

by varying the torque Σ we can therefore encompass both the cases $u_\theta(l(t),t) = 0$, so that the end is clamped and additional internal stresses will be generated, and $\bar{\sigma}_{s\theta}(l(t),t) = 0$, so the end of the cell is stress free, but a non-zero azimuthal velocity will be generated. The longitudinal tension generated in the cell wall is determined via a force balance on the end of the cell, that is the pressure acting on the (rigid) end plate of the cell must balance the tension normal to the plate in the sidewalls and the external compressive force, viz

$$\frac{R(P-Q)}{2} = \Delta\bar{\sigma}_{ss} \quad \text{on} \quad s = l(t). \tag{2.24}$$

Finally, the *a priori* unknown length of the cell satisfies

$$u_s(l(t),t) = \frac{\mathrm{d}l}{\mathrm{d}t}. \tag{2.25}$$

2.4. *Summary*

We therefore have 12 equations (2.9), (2.11)–(2.13), (2.15) and (2.18) for the 12 unknowns u_s, u_θ, v_s, v_θ, v_n, $\bar{\sigma}_{ss}$, $\bar{\sigma}_{s\theta}$, $\bar{\sigma}_{\theta\theta}$, R, h, ϕ, ρ. This system is 11th order in space and 4th order in time, and is subject to boundary conditions (2.20)–(2.24) and four initial conditions (2.19*a–d*). The 13th unknown, $l(t)$, is determined by the first-order ODE found from the additional boundary condition (2.25), with initial condition (2.19*e*). This therefore defines a closed system for the pressure-driven flow of a thin-walled anisotropic viscous axisymmetric sheet. The azimuthal and normal components of the centre-surface velocity, v_θ, v_n, decouple; v_n may be determined from (2.9*a*) once R and v_s are known, while the combination (2.9*c*) and (2.20*d*) gives $v_\theta = 0$. The normal centre-surface velocity, v_n, may be eliminated from (2.9*b*) using (2.9*a*), to find

$$\kappa_s \frac{\partial R}{\partial t} = \kappa_s v_s \frac{\partial R}{\partial s} - R\kappa_\theta \frac{\partial v_s}{\partial s} \tag{2.26}$$

when $\kappa_s \neq 0$, or from (2.9*a*) directly

$$\frac{\partial v_s}{\partial s} = 0, \tag{2.27}$$

if $\kappa_s = 0$. Thus the system reduces to 11 unknowns.

Unlike the case for a purely Newtonian fluid (VHO), the velocity of the centre-surface, $\boldsymbol{v}$, does not decouple from the governing equations; v_s appears explicitly in (2.13) and (2.15).

To further simplify the system we integrate (2.12*b,c*) with respect to s and apply conditions (2.23), (2.24) to find, for $0 \leqslant s \leqslant l(t)$,

$$\bar{\sigma}_{ss}(s,t) = \frac{(P-Q)R}{2\Delta}, \quad \bar{\sigma}_{s\theta}(s,t) = \frac{\Sigma}{R^2}. \tag{2.28}$$

3. Simplifications of the model

We now consider different simplifications of the model. As the cell wall is observed not to get significantly thinner during elongation, we pick $F(s,t)$ in (2.11) to ensure a solution in which $h = 1$. This function may be determined once R and u_s have been found. Similarly, we pick $G(s,t)$ in (2.15) to ensure a solution in which $\rho = 1$, so the fibre density remains constant. This eliminates two further unknowns, and leaves (2.12), (2.13), (2.18), (2.25) and (2.27) for the nine unknowns u_s, u_θ, v_s, $\bar{\sigma}_{ss}$, $\bar{\sigma}_{s\theta}$, $\bar{\sigma}_{\theta\theta}$, R, ϕ and l.

In § 3.1 we consider purely horizontal fibres (in a vertical cell), with no stretching in the fibre direction to leading order. In § 3.2 we extend this to small fibre angle. Finally, in § 3.3 we consider inextensibility in the fibre direction, for general fibre angle. Each case leads to a substantial simplification of the governing equations.

3.1. *Case 1: horizontal fibres*

If the fibres are initially horizontal, $\phi = 0$ satisfies (2.13) identically, so the fibres remain horizontal for $t > 0$. As v_s appears only in (2.13), this reduces the unknowns in the system by two to seven. Therefore we must solve (2.12) and (2.25) where, from

(2.18) with $a_\theta = 1$, $a_s = 0$,

$$\bar{\sigma}_{ss} = \mu_0 \frac{2}{R}\left(2R\frac{\partial u_s}{\partial s} + \frac{\mathrm{D}R}{\mathrm{D}t}\right), \tag{3.1a}$$

$$\bar{\sigma}_{s\theta} = (\mu_0 + \mu_3)\left(\frac{\partial u_\theta}{\partial s} - \frac{u_\theta}{R}\frac{\partial R}{\partial s}\right), \tag{3.1b}$$

$$\bar{\sigma}_{\theta\theta} = 2\mu_0\frac{\partial u_s}{\partial s} + \mu_1 + (4\mu_0 + \mu_2 + 4\mu_3)\frac{1}{R}\frac{\mathrm{D}R}{\mathrm{D}t}. \tag{3.1c}$$

Because u_θ decouples, appearing only in (3.1*b*), we may integrate the combination (2.28*b*) and (3.1*b*) with respect to s and apply conditions (2.20*b*) and set $u_\theta = 0$ or $\bar{\sigma}_{s\theta} = 0$ on $s = 0$ to find $u_\theta = 0$ (and hence $\bar{\sigma}_{s\theta} = 0$ also) identically; no azimuthal velocity is induced by the presence of the fibres (in the absence of an external torque). Thus the system is simplified to five unknowns, satisfying (2.12*a,b*), (2.25) and (3.1*a,c*).

With little experimental data on the relevant viscosities, we make a hypothesis about their relative sizes. Since plant cells expand longitudinally within the root expansion zone and display minimal radial expansion (see figure 1), we would like a solution in which R remains roughly constant, maintained by a large azimuthal tension $\bar{\sigma}_{\theta\theta}$ balancing the internal pressure. We therefore take $\mu_2 + 4\mu_3$ (proportional to $\mu_\parallel^* - \mu_\perp^*$) to be large so that $R = 1$ to leading order in (3.1*c*). Noticing that μ_2 and μ_3 appear only in the combination $\mu_2 + 4\mu_3$ in what follows, we take $\mu_2 + 4\mu_3 = \nu M(s,t)$, where $\nu \gg 1$ and $M(s,t)$ is an $O(1)$ function. We must ensure, however, that our original expansion performed in §2 remains valid. If ν is taken to be so large that $\epsilon\nu$ is $O(1)$, then $O(\epsilon)$ terms in the expansion of strain rate (Appendix B.1) will enter the $O(1)$ expansion of the stress tensor (2.18) which are currently neglected. We therefore require $\epsilon \ll 1/\nu \ll 1$.

We rescale $\bar{\sigma}_{\theta\theta} = \nu\tilde{\sigma}_{\theta\theta}$ and construct a regular expansion in powers of small $1/\nu$ such that $R = R^{(0)} + R^{(1)}/\nu + \cdots$. At leading order in $1/\nu$, from (2.12*a*) and (3.1*c*) (where $\mathrm{D}^{(0)}/\mathrm{D}t \equiv \partial/\partial t + u_s^{(0)}\partial/\partial s$)

$$\kappa_\theta^{(0)}\tilde{\sigma}_{\theta\theta}^{(0)} = 0, \quad \tilde{\sigma}_{\theta\theta}^{(0)} = \frac{M(s,t)}{R^{(0)}}\frac{\mathrm{D}^{(0)}R^{(0)}}{\mathrm{D}t} \tag{3.2}$$

along with (2.11), (2.12*b*) and (2.18*a*) applied to leading-order quantities. Using (3.2) we find

$$\tilde{\sigma}_{\theta\theta}^{(0)} = 0, \qquad \frac{\mathrm{D}^{(0)}R^{(0)}}{\mathrm{D}t} = 0, \tag{3.3}$$

and we choose $F(s,t)$ in (2.11) to be $R^{(0)}\,\partial u_s^{(0)}/\partial s$ to ensure $h^{(0)} = 1$. Therefore (3.1*a*) reduces to

$$\bar{\sigma}_{ss}^{(0)} = 4\mu_0(s,t)\frac{\partial u_s^{(0)}}{\partial s}. \tag{3.4}$$

This is equivalent to the usual Trouton (1906) model for extensional flow; the fibres resist radial changes but the matrix viscosity controls axial expansion.

Expanding (2.28*b*) we find

$$\bar{\sigma}_{ss}^{(0)} = \frac{(P - Q)\,R^{(0)}}{2\Delta^{(0)}}, \tag{3.5}$$

where $\Delta^{(0)} = (1 - (\partial R^{(0)}/\partial s)^2)^{1/2}$, leaving us to solve a nonlinear hyperbolic PDE for $R^{(0)}$ given by (3.3*b*) with

$$\frac{\partial u_s^{(0)}}{\partial s} = \frac{(P-Q)\,R^{(0)}}{8\mu_0(s,t)\,\Delta^{(0)}}. \tag{3.6}$$

This gives the evolution from a general initial condition for R. When $R(s,0) = 1$, as in (2.19), (3.3*b*) has the simple solution $R^{(0)} = 1$, which immediately gives

$$v_s^{(0)} = v_\theta^{(0)} = v_n^{(0)} = 0, \tag{3.7}$$

from (2.9). We may therefore integrate (3.6) with respect to s to find

$$u_s^{(0)} = \frac{(P-Q)}{8}\int_0^s \frac{1}{\mu_0(s,t)}\,\mathrm{d}s. \tag{3.8}$$

Finally, applying boundary condition (2.25) for the leading-order unknown length of the cell, $l^{(0)}$, we find

$$\frac{\mathrm{d}l^{(0)}}{\mathrm{d}t} = \frac{(P-Q)}{8}\int_0^{l^{(0)}} \frac{1}{\mu_0(s,t)}\,\mathrm{d}s. \tag{3.9}$$

Thus, we have an ODE for the growing cell length depending on the internal turgor pressure $P(t)$, the external compression Q and the matrix viscosity $\mu_0(s,t)$.

At next order in $1/\nu$ in (2.12*a*) and (3.1*a*), we find (assuming $\mu_1 = O(1)$)

$$\kappa_s^{(0)}\bar{\sigma}_{ss}^{(0)} + \kappa_\theta^{(0)}\tilde{\sigma}_{\theta\theta}^{(1)} + \kappa_\theta^{(1)}\tilde{\sigma}_{\theta\theta}^{(0)} = P, \tag{3.10}$$

$$\tilde{\sigma}_{\theta\theta}^{(1)} = M(s,t)\frac{1}{R^{(0)}}\frac{\mathrm{D}^{(0)}R^{(1)}}{\mathrm{D}t} + 2\mu_0\frac{\partial u_s^{(0)}}{\partial s} + \mu_1, \tag{3.11}$$

which reduces to

$$\frac{\mathrm{D}^{(0)}R^{(1)}}{\mathrm{D}t} = \frac{1}{M(s,t)}\left(\frac{3P}{4} - \mu_1 + \frac{Q}{4}\right), \tag{3.12}$$

upon substituting for the leading-order expressions (note $\kappa_s^{(0)} = 0$, $\kappa_\theta^{(0)} = 1/R^{(0)}$). This shows that growth or shrinkage of the cell during elongation is governed by the relative sizes of μ_1, which is related to the pre-stress in the fibres, the transmural pressure difference P and the external compression Q. When P is sufficiently large, the cell will expand radially; $\mu_2 + 4\mu_3$ will influence the speed of this radius change, whereas the matrix viscosity μ_0 affects the longitudinal velocity $u_s^{(0)}$.

If we assume $\mu_0 = \mu_0(t)$, we recover a simple version of (1.2)

$$u_s^{(0)} = \frac{(P-Q)}{8\mu_0}s, \qquad \frac{\mathrm{d}l^{(0)}}{\mathrm{d}t} = \frac{(P-Q)}{8\mu_0(t)}l^{(0)}, \tag{3.13}$$

giving

$$l^{(0)}(t) = l_0\exp\left(\frac{(P-Q)}{8}\int_0^t \frac{1}{\mu_0(t)}\,\mathrm{d}t\right), \tag{3.14}$$

where l_0 is the initial length of the cell.

If, in addition, the fibre properties do not vary during growth, so that $M(s,t) = 1$, and μ_1 is constant, (3.12) gives (assuming $R^{(1)} = 0$ at $t = 0$)

$$R^{(1)}(s,t) = t\left(\frac{3P}{4} - \mu_1 + \frac{Q}{4}\right), \tag{3.15}$$

for the majority of the cell length. Near $s=0,\ l$ there will be boundary layers in which we expect the curvature term κ_s (containing a second derivative of R in s) to become important, allowing the radius to adjust to satisfy $R^{(1)}=0$ at $s=0,\ l$. We do not consider this inner problem here. We discuss the significance of the predictions of this simple form of the model, particularly (3.13) and (3.14), in § 4 below.

3.2. *Case 2: small fibre angle*

We now consider the case of small, but non-zero, fibre angle. Of course ϕ, while starting small, may not remain so, but considering this case gives insight into the less tractable case $\phi=O(1)$. We return to the system of nine unknowns discussed at the start of § 3, again taking μ_2 or μ_3 to be large to resist changes in radius as the cell expands.

We set $\phi=\delta\tilde{\phi}$, for $\delta=\phi_0\ll 1$ such that $\tilde{\phi}=1$ at $t=0$, taking $\tilde{\phi}=O(1)$; we also rescale $u_\theta=\delta\tilde{u}_\theta$ in order to find the non-zero induced azimuthal velocity. We shall investigate different magnitudes of δ in comparison to μ_2 and μ_3 shortly; as before we must take care not to violate the original asymptotic expansion in ϵ. Taylor-expanding a_θ and a_s in small δ yields $a_\theta=1-\delta^2\tilde{\phi}^2/2+\cdots$, $a_s=\delta\tilde{\phi}-\delta^3\tilde{\phi}^3/6+\cdots$, and we construct a regular expansion in δ of the form $R=R^{(0)}+\delta^2R^{(1)}+\cdots$. Thus we express integrated stresses (2.18) as

$$\bar{\sigma}_{ss}=\frac{2}{R^{(0)}}\mu_0\left(2R^{(0)}\frac{\partial u_s^{(0)}}{\partial s}+\frac{\mathrm{D}^{(0)}R^{(0)}}{\mathrm{D}t}\right)+\mu_1\delta^2\tilde{\phi}^{(0)2}+\mu_2\delta^2\tilde{\phi}^{(0)2}\left(\zeta^{(0)}+\delta^2\zeta^{(1)}\right)$$
$$+4\mu_3\delta^2\tilde{\phi}\left(\frac{1}{2}\left(\frac{\partial\tilde{u}_\theta^{(0)}}{\partial s}-\frac{\tilde{u}_\theta^{(0)}}{R^{(0)}}\frac{\partial R^{(0)}}{\partial s}\right)+\tilde{\phi}\frac{\partial u_s^{(0)}}{\partial s}\right)+\cdots, \tag{3.16a}$$

$$\bar{\sigma}_{s\theta}=\mu_0\delta\left(\frac{\partial\tilde{u}_\theta^{(0)}}{\partial s}-\frac{\tilde{u}_\theta^{(0)}}{R^{(0)}}\frac{\partial R^{(0)}}{\partial s}\right)+\mu_1\delta\tilde{\phi}^{(0)}+\mu_2\delta\tilde{\phi}^{(0)}\left(1-\frac{\delta^2\tilde{\phi}^{(0)2}}{2}\right)\left(\zeta^{(0)}+\delta^2\zeta^{(1)}\right)$$
$$+2\mu_3\delta\left(\frac{1}{2}\left(\frac{\partial\tilde{u}_\theta^{(0)}}{\partial s}-\frac{\tilde{u}_\theta^{(0)}}{R^{(0)}}\frac{\partial R^{(0)}}{\partial s}\right)+\frac{\tilde{\phi}^{(0)}}{R^{(0)}}\left(\frac{\mathrm{D}^{(0)}R^{(0)}}{\mathrm{D}t}+R^{(0)}\frac{\partial u_s^{(0)}}{\partial s}\right)\right)+\cdots, \tag{3.16b}$$

$$\bar{\sigma}_{\theta\theta}=\frac{2}{R^{(0)}}\mu_0\left(R^{(0)}\frac{\partial u_s^{(0)}}{\partial s}+2\frac{\mathrm{D}^{(0)}R^{(0)}}{\mathrm{D}t}\right)+\mu_1+\mu_2\left(1-\delta^2\tilde{\phi}^{(0)2}\right)\left(\zeta^{(0)}+\delta^2\zeta^{(1)}\right)$$
$$+4\mu_3\left(\frac{1}{R^{(0)}}\frac{\mathrm{D}^{(0)}R^{(0)}}{\mathrm{D}t}+\delta^2\left(\frac{1}{R^{(0)}}\left(\frac{\mathrm{D}^{(0)}R^{(1)}}{\mathrm{D}t}+u_s^{(1)}\frac{\partial R^{(0)}}{\partial s}\right)-\frac{\tilde{\phi}^{(0)2}}{R^{(0)}}\frac{\mathrm{D}^{(0)}R^{(0)}}{\mathrm{D}t}\right)\right.$$
$$\left.+\frac{\tilde{\phi}^{(0)}}{2}\left(\frac{\partial\tilde{u}_\theta^{(0)}}{\partial s}-\frac{\tilde{u}_\theta^{(0)}}{R^{(0)}}\frac{\partial R^{(0)}}{\partial s}\right)\right)+\cdots, \tag{3.16c}$$

the evolution equation for the director field (2.13) as

$$\frac{\partial\tilde{\phi}^{(0)}}{\partial t}+\left(u_s^{(0)}+v_s^{(0)}\right)\frac{\partial\tilde{\phi}^{(0)}}{\partial s}=\tilde{\phi}^{(0)}\left(\frac{\partial u_s^{(0)}}{\partial s}-\frac{1}{R^{(0)}}\frac{\mathrm{D}^{(0)}R^{(0)}}{\mathrm{D}t}\right)+\cdots, \tag{3.17}$$

and the relative length change of fibres (2.14) as

$$\begin{aligned}\zeta &= \zeta^{(0)} + \delta^2\zeta^{(1)} + \cdots,\\ &= \frac{1}{R^{(0)}}\frac{\mathrm{D}^{(0)}R^{(0)}}{\mathrm{D}t} + \delta^2\left(\frac{1}{R^{(0)}}\left(\frac{\mathrm{D}^{(0)}R^{(1)}}{\mathrm{D}t} + u_s^{(1)}\frac{\partial R^{(0)}}{\partial s}\right) - \frac{\tilde{\phi}^{(0)2}}{R^{(0)}}\frac{\mathrm{D}^{(0)}R^{(0)}}{\mathrm{D}t}\right.\\ &\quad\left. + \tilde{\phi}^{(0)}\left(\frac{\partial \tilde{u}_\theta^{(0)}}{\partial s} - \frac{\tilde{u}_\theta^{(0)}}{R^{(0)}}\frac{\partial R^{(0)}}{\partial s} + \tilde{\phi}^{(0)}\frac{\partial u_s^{(0)}}{\partial s}\right)\right) + \cdots. \end{aligned} \tag{3.18}$$

We have retained terms past leading order in (3.16)–(3.18) in places where the leading-order terms turn out to be identically zero. These expressions, along with the original governing equations (2.11) and (2.12) and the expression (2.27) for the axial velocity of the moving coordinate frame, define the system to be solved, subject to initial and boundary conditions (2.19)–(2.25).

From (2.12*a*) and (3.16*c*) we again see that if we take $\mu_2 + 4\mu_3$ to be large the cell will resist changes in radius. However, unlike the case with horizontal fibres, μ_2 and μ_3 do not appear just in this combination. We can therefore take either (or both) of these quantities to be large. To retain the order of the original expansion, we still require $\epsilon \ll \{1/\mu_2, 1/\mu_3\} \ll 1$ as in § 3.1, from which we recover (3.3*b*).

Therefore (3.17) becomes

$$\frac{\partial \tilde{\phi}^{(0)}}{\partial t} + \left(u_s^{(0)} + v_s^{(0)}\right)\frac{\partial \tilde{\phi}^{(0)}}{\partial s} = \tilde{\phi}^{(0)}\frac{\partial u_s^{(0)}}{\partial s} \tag{3.19}$$

along with (2.28) applied to leading-order quantities. The lowest-order terms (in δ) in the expansion of $\bar{\sigma}_{ss}$, $\bar{\sigma}_{s\theta}$ are given by

$$\begin{aligned}\bar{\sigma}_{ss} &= 4\mu_0\frac{\partial u_s^{(0)}}{\partial s} + \mu_1\delta^2\tilde{\phi}^{(0)2} + \mu_2\delta^4\tilde{\phi}^{(0)2}\zeta^{(1)}\\ &\quad + 4\mu_3\delta^2\tilde{\phi}\left(\frac{1}{2}\left(\frac{\partial \tilde{u}_\theta^{(0)}}{\partial s} - \frac{\tilde{u}_\theta^{(0)}}{R^{(0)}}\frac{\partial R^{(0)}}{\partial s}\right) + \tilde{\phi}\frac{\partial u_s^{(0)}}{\partial s}\right) + \cdots, \end{aligned} \tag{3.20a}$$

$$\begin{aligned}\bar{\sigma}_{s\theta} &= \mu_0\delta\left(\frac{\partial \tilde{u}_\theta^{(0)}}{\partial s} - \frac{\tilde{u}_\theta^{(0)}}{R^{(0)}}\frac{\partial R^{(0)}}{\partial s}\right) + \mu_1\delta\tilde{\phi}^{(0)} + \mu_2\delta^3\tilde{\phi}^{(0)}\zeta^{(1)}\\ &\quad + 2\mu_3\delta\left(\frac{1}{2}\left(\frac{\partial \tilde{u}_\theta^{(0)}}{\partial s} - \frac{\tilde{u}_\theta^{(0)}}{R^{(0)}}\frac{\partial R^{(0)}}{\partial s}\right) + \tilde{\phi}^{(0)}\frac{\partial u_s^{(0)}}{\partial s}\right) + \cdots, \end{aligned} \tag{3.20b}$$

where $\zeta^{(1)}$ is given by

$$\zeta^{(1)} = \frac{1}{R^{(0)}}\left(\frac{\mathrm{D}^{(0)}R^{(1)}}{\mathrm{D}t} + u_s^{(1)}\frac{\partial R^{(0)}}{\partial s}\right) + \tilde{\phi}^{(0)}\left(\frac{\partial \tilde{u}_\theta^{(0)}}{\partial s} - \frac{\tilde{u}_\theta^{(0)}}{R^{(0)}}\frac{\partial R^{(0)}}{\partial s} + \tilde{\phi}^{(0)}\frac{\partial u_s^{(0)}}{\partial s}\right) \tag{3.21}$$

from (3.18). Since $R^{(1)}$ and $u_s^{(1)}$ appear within (3.21) we must go to next order to close the model. However, when $R = 1$ initially, $R^{(0)} = 1$ from (3.3*b*) and hence $u_s^{(1)}$ decouples, no longer appearing in (3.21). The slow creep of the cell radius, $R^{(1)}$, is determined from the next-order terms within (2.12*a*) and (3.16*c*).

It is useful to scale $\{\bar{\sigma}_{s\theta}, \Sigma\} = \{\tilde{\sigma}_{s\theta}, \tilde{\Sigma}\}/\delta$ so that μ_1, μ_2, μ_3 and δ appear in the same combinations in (3.20*a*) and the rescaled (3.20*b*). Combining (2.12*a*) and (2.28)

with (3.16*c*) and (3.20) we find

$$P = 2\mu_0 \frac{\partial u_s^{(0)}}{\partial s} + \mu_1 + \mu_2 \delta^2 \zeta^{(1)} + 4\mu_3 \delta^2 \left(\frac{\mathrm{D}^{(0)} R^{(1)}}{\mathrm{D}t} + \frac{\tilde{\phi}^{(0)}}{2} \frac{\partial \tilde{u}_\theta^{(0)}}{\partial s} \right), \tag{3.22a}$$

$$\frac{P-Q}{2} = 4\mu_0 \frac{\partial u_s^{(0)}}{\partial s} + \delta^2 \tilde{\phi}^{(0)^2} \left(\mu_1 + \mu_2 \delta^2 \zeta^{(1)} \right) + 4\mu_3 \delta^2 \tilde{\phi} \left(\frac{1}{2} \frac{\partial \tilde{u}_\theta^{(0)}}{\partial s} + \tilde{\phi} \frac{\partial u_s^{(0)}}{\partial s} \right), \tag{3.22b}$$

$$\tilde{\Sigma} = \mu_0 \delta^2 \frac{\partial \tilde{u}_\theta^{(0)}}{\partial s} + \delta^2 \tilde{\phi}^{(0)} \left(\mu_1 + \mu_2 \delta^2 \zeta^{(1)} \right) + 2\mu_3 \delta^2 \left(\frac{1}{2} \frac{\partial \tilde{u}_\theta^{(0)}}{\partial s} + \tilde{\phi}^{(0)} \frac{\partial u_s^{(0)}}{\partial s} \right), \tag{3.22c}$$

where

$$\zeta^{(1)} = \frac{\mathrm{D}^{(0)} R^{(1)}}{\mathrm{D}t} + \tilde{\phi}^{(0)} \left(\frac{\partial \tilde{u}_\theta^{(0)}}{\partial s} + \tilde{\phi}^{(0)} \frac{\partial u_s^{(0)}}{\partial s} \right), \tag{3.23}$$

from (3.21).

We wish to investigate distinguished limits in which the maximum number of terms within (3.22) appear. Clearly we should take $\mu_1 = O(\mu_2 \delta^2)$, $\mu_3 \delta^2 = O(1)$, but the choice of size for μ_2 is less clear; $\mu_2 \delta^2$ appears in (3.22*a*) whereas $\mu_2 \delta^4$ appears in (3.22*b*) and (3.22*c*). When $\mu_2 \delta^2 = O(1)$ all terms appear within (3.22*a*), but the μ_1 and μ_2 terms within (3.22*b*) and (3.22*c*) are $O(\delta^2)$. When $\mu_2 \delta^4 = O(1)$, however, the μ_1 and μ_2 terms dominate within (3.22*a*), and hence $\mu_1 + \delta^2 \mu_2 \zeta^{(1)} = 0$ (implying high resistance to stretching in the fibre direction), removing the dependence on μ_1, μ_2 within (3.22*b*) and (3.22*c*) as well. We therefore take $\mu_0 = O(1)$, $\mu_1 = O(1)$, $\mu_2 \delta^2 = M_2$, $\mu_3 \delta^2 = M_3$ where M_2, M_3 are order one functions; the limits $M_1 \to \infty$, $M_2 \to \infty$ capture the case $\mu_1 \delta^2 = O(1)$, $\mu_2 \delta^4 = O(1)$

Assuming μ_0, μ_1, M_2, M_3, ϕ_0, R_0 have no spatial dependence, with $R^{(0)} = 1$, we find (3.7) and

$$\frac{\mathrm{d}\tilde{\phi}^{(0)}}{\mathrm{d}t} = \tilde{\phi}^{(0)} \frac{\partial u_s^{(0)}}{\partial s}. \tag{3.24}$$

As in the case for $R^{(1)}$ in § 3.1, we take $\tilde{\phi}$ to be only a function of time, neglecting the region over which it adjusts from $\phi = \phi_0$ at $s = 0$. This inner problem is expected to have little effect on the overall dynamics. Integrating (3.22*b*) and (3.22*c*) with respect to s, and solving the resulting simultaneous equations for $u_s^{(0)}$ and $\tilde{u}_\theta^{(0)}$, we find (in terms of the unknown $\tilde{\phi}^{(0)}(t)$)

$$u_s^{(0)} = \frac{P - Q - 4\tilde{\Sigma}\tilde{\phi}^{(0)}}{8\mu_0} s, \tag{3.25a}$$

$$\tilde{u}_\theta^{(0)} = \frac{4\left(\mu_0 + M_3 \tilde{\phi}^{(0)^2}\right)\tilde{\Sigma} - M_3 \tilde{\phi}^{(0)} (P - Q)}{4\mu_0 M_3} s. \tag{3.25b}$$

Finally, applying (2.25) to (3.25*a*) we find

$$\frac{1}{l^{(0)}} \frac{\mathrm{d}l^{(0)}}{\mathrm{d}t} = \frac{P - Q - 4\tilde{\Sigma}\tilde{\phi}^{(0)}}{8\mu_0}. \tag{3.26}$$

This is a modified Lockhart-type equation incorporating the effects of non-zero fibre angle. When $\tilde{\phi} = 0$ or $\tilde{\Sigma} = 0$ we regain the original expression (3.13*b*); (3.26) shows how torque on the end plates can amplify the effects of small fibre tilt to have a leading-order influence on the cell's rate of extension.

Substituting (3.25) into (3.22*a*) and rearranging, we find a PDE for $R^{(1)}$, also in terms of the unknown $\tilde{\phi}^{(0)}$,

$$(M_2+4M_3)\frac{\mathrm{D}^{(0)}R^{(1)}}{\mathrm{D}t} = P\left(\frac{3}{4}+\frac{M_2+4M_3}{8\mu_0}\tilde{\phi}^{(0)2}\right)-\mu_1+Q\left(\frac{1}{4}-\frac{(M_2+4M_3)\tilde{\phi}^{(0)2}}{8\mu_0}\right)$$
$$-\left(2\mu_0(M_2+M_3)+(M_2+4M_3)M_3\tilde{\phi}^{(0)2}\right)\frac{\tilde{\phi}^{(0)}\tilde{\Sigma}}{2\mu_0 M_3}, \tag{3.27}$$

again neglecting boundary layers near $s=0, l$. This equation reduces to (3.12) when $\tilde{\phi}=0$, noting $M_2+4M_3=M$. From (3.27), we see that the external torque can be used to suppress radius changes, by choosing Σ such that the right-hand side is equal to zero.

Using (2.25) and (3.24), $l^{(0)}$ and $\phi^{(0)}$ may be related via

$$\frac{\mathrm{d}l^{(0)}}{\mathrm{d}t} = \int_0^{l^{(0)}}\frac{\partial u_s^{(0)}}{\partial s}\,\mathrm{d}s = \frac{l^{(0)}}{\tilde{\phi}^{(0)}}\frac{\mathrm{d}\tilde{\phi}^{(0)}}{\mathrm{d}t}, \tag{3.28}$$

and hence

$$\tilde{\phi}^{(0)}(t) = l^{(0)}/l_0. \tag{3.29}$$

Therefore (3.26) may be written as a nonlinear ODE for the unknown length $l^{(0)}$. We rescale $\hat{l}=l^{(0)}/l_0$ to find

$$\frac{1}{\hat{l}}\frac{\mathrm{d}\hat{l}}{\mathrm{d}t} = \frac{P-Q-4\tilde{\Sigma}\hat{l}}{8\mu_0}, \tag{3.30a}$$

$$(M_2+4M_3)\frac{\mathrm{D}^{(0)}R^{(1)}}{\mathrm{D}t} = P\left(\frac{3}{4}+\frac{M_2+4M_3}{8\mu_0}\hat{l}^2\right)-\mu_1+Q\left(\frac{1}{4}-\frac{(M_2+4M_3)\hat{l}^2}{8\mu_0}\right)$$
$$-\left(2\mu_0(M_2+M_3)+(M_2+4M_3)M_3\hat{l}^2\right)\frac{\hat{l}\tilde{\Sigma}}{2\mu_0 M_3}. \tag{3.30b}$$

The cell length may be determined from (3.30*a*), whence the slow radius evolution may be found from (3.30*b*). Predictions from (3.30) are illustrated in § 4. An extension of (3.30*a*) to incorporate variation of fibre direction across the wall is given in Appendix D.

3.3. *Case 3: Inextensibility in the fibre direction*

We now consider the material to be inextensible in the fibre direction, that is we take $\mu_2\to\infty$, $\zeta=a_ia_je_{ij}\to 0$ in (2.18) with $\mu_2 a_ia_je_{ij}=\hat{T}$ where $\hat{T}$ is the $O(1)$ tension along the fibres which enforces inextensibility. In contrast to § 3.2, we no longer assume that the fibre angle is small. We return to the system of nine unknowns described at the start of § 3. The non-dimensional stress tensor (2.4) becomes

$$\sigma_{ij} = -p\delta_{ij}+2\mu_0 e_{ij}+Ta_ia_j+2\mu_3\left(a_ia_le_{jl}+a_ja_me_{mi}\right), \tag{3.31}$$

where $T=\mu_1+\hat{T}$, absorbing the pre-stress within the fibres into the tension induced by inextensibility.

In §§ 3.1 and 3.2, we found a solution for zero and small fibre angle in which the cell radius is constant for large μ_2 and for which u_s, u_θ depend linearly on s, when we take no spatial dependence within μ_0, μ_1, μ_2, μ_3, ϕ_0. We therefore look for a similarity solution in which these effects are assumed. We impose $R=1$ through the appropriate

choice of Σ (as suggested by (3.27)); while to some degree this is artificial, it allows the finite-angle case to be addressed directly. This simplifies (2.12*a*) and (2.28*a*) to

$$\bar{\sigma}_{\theta\theta} = P, \quad \bar{\sigma}_{ss} = (P - Q)/2, \tag{3.32}$$

and retains (2.28*b*). We assume uniform axial stretching and twisting, that is

$$(u_\theta, u_s) = E(t)(\cos\alpha, \sin\alpha)\, s \tag{3.33}$$

for some $E(t)$, where α gives the direction of stretching. Substituting (3.33) into (2.13), (2.14), (2.25), (3.31) we find

$$\frac{1}{l}\frac{\mathrm{d}l}{\mathrm{d}t} = E\sin\alpha, \tag{3.34a}$$

$$\zeta = 0 = E\sin\phi\cos(\alpha - \phi), \tag{3.34b}$$

$$\frac{\mathrm{d}\phi}{\mathrm{d}t} = E\sin\phi\sin(\alpha - \phi), \tag{3.34c}$$

$$\bar{\sigma}_{ss} = 4\mu_0 E\sin\alpha + T\sin^2\phi + 4\mu_3 E\left(\sin^2\phi\sin\alpha + \frac{\sin\phi\cos\phi\cos\alpha}{2}\right), \tag{3.34d}$$

$$\bar{\sigma}_{s\theta} = \mu - 0E\cos\alpha + T\sin\phi\cos\phi + \mu_3(E\cos\alpha + 2E\sin\phi\cos\phi\sin\alpha), \tag{3.34e}$$

$$\bar{\sigma}_{\theta\theta} = 2\mu_0 E\sin\alpha + T\cos^2\phi + 4\mu_3\frac{E\sin\phi\cos\phi\cos\alpha}{2}. \tag{3.34f}$$

Using (3.32), (3.34*d*) and (3.34*f*) we solve the resulting simultaneous equations for E and T to find

$$T = \frac{2(3\mu_0\sin\alpha + \mu_3(4\sin^2\phi\sin\alpha + \sin\phi\cos\phi\cos\alpha))E + Q}{3\cos^2\phi - 2}, \tag{3.35a}$$

$$E = \frac{(3/2\cos^2\phi - 1)P - 1/2\cos^2\phi\, Q}{(2\mu_0\sin\alpha(3\cos^2\phi - 1) + 2\mu_3\sin\phi\cos\phi(2\sin\phi\cos\phi\sin\alpha + (2\cos^2\phi - 1)\cos\alpha))}. \tag{3.35b}$$

The appropriate choice of Σ to impose zero radius change is therefore of the form

$$\Sigma = \mu_0 E\cos\alpha + T\sin\phi\cos\phi + \mu_3 E(\cos\alpha + 2\sin\phi\cos\phi\sin\alpha), \tag{3.36}$$

from (2.28*b*) and (3.34*e*). From (3.34*b*) there are three possibilities to ensure zero extension in the fibre direction; $E = 0$, $\sin\phi = 0$ or $\cos(\phi - \alpha) = 0$. When $E = 0$, equivalent from (3.35*b*) to $\phi = \phi_c$ where (assuming $Q < P$)

$$\cos\phi_c = \sqrt{2P/(3P - Q)}, \tag{3.37}$$

there is no growth of the cell. When $\phi = 0$, we regain the system considered in § 3.1. We therefore consider the case $\cos(\phi - \alpha) = 0$. Since we expect $0 < \phi < \pi/2$ and $\sin\alpha > 0$ (so $u_s > 0$), we take $\alpha = \phi + \pi/2$. Thus we find

$$\frac{1}{l}\frac{\mathrm{d}l}{\mathrm{d}t} = E\cos\phi, \tag{3.38a}$$

$$\frac{\mathrm{d}\phi}{\mathrm{d}t} = E\sin\phi, \tag{3.38b}$$

$$T = \frac{3(\mu_0 + \mu_3\sin^2\phi)P + (\mu_0 - \mu_3\sin^2\phi)Q}{2(\mu_0(3\cos^2\phi - 1) + \mu_3\sin^2\phi)}, \tag{3.38c}$$

$$E = \frac{(3\cos^2\phi - 2)P - \cos^2\phi\, Q}{4\cos\phi(\mu_0(3\cos^2\phi - 1) + \mu_3\sin^2\phi)}, \tag{3.38d}$$

from (3.34*a*), (3.34*c*), and (3.35). Combining (3.38*a*) and (3.38*d*) and taking $\phi = 0$ regains (3.13*b*). Equations (3.38*b*) and (3.38*d*) reduce to a single nonlinear ODE for the fibre angle, ϕ,

$$\frac{\mathrm{d}\phi}{\mathrm{d}t} = \frac{((3\cos^2\phi - 2)P - \cos^2\phi\, Q)\sin\phi}{4\cos\phi(\mu_0(3\cos^2\phi - 1) + \mu_3\sin^2\phi)}. \tag{3.39}$$

We now consider the cell length. Eliminating E from (3.38*a*) and (3.38*b*) (assuming $\phi_0 \neq 0$), we find

$$\frac{l}{l_0} = \frac{\sin\phi}{\sin\phi_0}, \tag{3.40}$$

which is equivalent to (3.29) for small fibre angle. Substituting (3.40) in (3.39) and rescaling $\hat{l} = \sin\phi_0 l/l_0$, we find

$$\frac{1}{\hat{l}}\frac{\mathrm{d}\hat{l}}{\mathrm{d}t} = \frac{(1 - 3\hat{l}^2)P - (1 - \hat{l}^2)Q}{4(\mu_0(2 - 3\hat{l}^2) + \mu_3\hat{l}^2)}. \tag{3.41}$$

Provided $0 < \phi_0 < \phi^\dagger$, where $\cos\phi^\dagger = \sqrt{(\mu_0 - \mu_3)/(3\mu_0 - \mu_3)}$, ϕ will tend to the steady state ϕ_c (see (3.37)) as $t \to \infty$. Likewise, for $Q < P$,

$$l \to \frac{l_0}{\sin\phi_0}\sqrt{\frac{P - Q}{3P - Q}} \tag{3.42}$$

for increasing time. This limit is independent of the mechanical properties of the wall; for a given initial fibre orientation the cell will grow to the same constant length in all cases.

Taking $\mu_0\,(=1$ without loss of generality) and μ_3 to be constant, we solve (3.39) to find

$$\left(\frac{\left(3\cos^2\phi - 2\right)P - \cos^2\phi\, Q}{\left(3\cos^2\phi_0 - 2\right)P - \cos^2\phi_0 Q}\right)^{\Upsilon}\frac{\cos^2\phi - 1}{\cos^2\phi_0 - 1} = \exp\left(\frac{(P - Q)\,t}{4}\right), \tag{3.43a}$$

where

$$\Upsilon \equiv \frac{-(3P + Q + \mu_3(P - Q))}{2(3P - Q)}, \tag{3.43b}$$

along with

$$\frac{\hat{l}^2}{\hat{l}_0^2}\left(\frac{P(3\hat{l}^2 - 1) - Q(\hat{l}^2 - 1)}{P(3\hat{l}_0^2 - 1) - Q(\hat{l}_0^2 - 1)}\right)^{\Upsilon} = \exp\left(\frac{(P - Q)t}{4}\right), \tag{3.43c}$$

where $\hat{l}_0 = \sin\phi_0$. Solutions (3.43*a*) and (3.43*c*) are discussed in § 4.

4. Results

In § 3 we derived the governing equations for anisotropic plant cell expansion for three simplifying sets of assumptions: horizontal fibres (i.e. perpendicular to the longitudinal axis of the cell, § 3.1), fibres with a small deviation from horizontal (§ 3.2) and complete inextensibility in the fibre direction (§ 3.3). It is straightforward to reduce both solutions found in §§ 3.2, 3.3 to that found in § 3.1 in the limit $\phi \to 0$, and we show how solutions in §§ 3.2 and 3.3 match up in limiting cases in Appendix C. We now discuss these results in more detail, in particular comparing them to the

Lockhart-type cell-growth equation (1.2) for turgor-pressure-induced growth, noting that we are considering the zero-yield limit.

Measuring the viscosity of the cell wall is experimentally very difficult, and few measurements are available in the literature. Those that do exist are tissue-scale measurements of many cells and are thus not an accurate reflection of the matrix viscosity described here. However, these measurements should give a rough order of magnitude to validate our model. Thompson (2001) (for tomato epidermal cells) and Tanimoto *et al.* (2000) (for the elongation zone of pea lateral roots) give tissue-scale extensional viscosity values of 10^9–$10^{11}\,\mathrm{kg\,m^{-1}\,s^{-1}}$. Within the *Arabidopsis* elongation zone, cells have a radius of approximately $10\,\mu$m (Swarup *et al.* 2005) and a cell-wall thickness of 70 nm (P. Derbyshire 2008, personal communication; similar measurements are reported for *Arabidopsis* hypocotyls in Derbyshire *et al.* 2007*a*) with a longitudinal pressure difference (i.e. $P^* - Q^*$) of approximately 1 bar. If the matrix viscosity is taken to be constant, the dimensional version of (3.14) may be written as an expression for this viscosity in terms of the more accurately known quantities, viz

$$\mu_0^* = \frac{(P^* - Q^*)R_0^* t^*}{8h^* \ln(l^*/l_0^*)}. \tag{4.1}$$

For the cell to grow in length approximately 30 times over a time scale of 6 h (i.e. setting $l^*/l_0^* = 30$, $t = 6$ h in (4.1)) gives a matrix viscosity of the order $10^{10}\,\mathrm{kg\,m^{-1}\,s^{-1}}$, which is similar to that found by Thompson (2001) and Tanimoto *et al.* (2000). From (2.8), these values equate to one non-dimensional time unit representing 800 s, and so the 6 h of growth through the elongation zone is equivalent to 30 non-dimensional time units.

When the fibres are initially horizontal they remain horizontal; a high elongational viscosity in the fibre direction restricts radial changes while allowing axial expansion. Our expression for the growing length of the cell, (3.13*b*), reduces to the zero-yield Lockhart-type cell-growth equation when the matrix viscosity is a function of time only. We can therefore identify the empirical 'extensibility' appearing in (1.2) and (1.3) of an individual cell in terms of fundamental quantities, that is

$$\Phi^* = \frac{1}{4\mu_0^*}, \quad \overline{\Phi}^* = \frac{R_0^*}{8\mu_0^* h_0^*}. \tag{4.2}$$

In this case, Φ^* depends only on the matrix viscosity of the cell wall; the fibre properties do not appear explicitly, although the effects of cross-links between CMF, and the presence of the fibres themselves, can be assumed to influence μ_0^*. The definition of extensibility often used in the literature ($\overline{\Phi}^*$) incorporates geometric factors which are explicit within our growth equation. As is evident from (3.14), when μ_0^* is constant the cell length l/l_0 when the fibres are horizontal increases exponentially if the turgor pressure P exceeds the external compressive force Q. Growth may be saturated if the matrix viscosity increases sufficiently rapidly with time, as illustrated in figure 3.

For small fibre angles ($\phi = O(\delta)$), we consider the canonical limit $\mu_1 = O(1)$, $\mu_2\delta^2 = O(1)$, $\mu_3\delta^2 = O(1)$, which contains the most leading-order effects. The large elongational viscosity ($\mu_2 + 4\mu_3$) again suppresses radial changes while allowing axial growth. When the viscosities, initial cell radius and fibre angle have no spatial dependence, the cell length is proportional to scaled fibre angle (3.29). Since the length of the cell increases approximately 30 fold over the length of the elongation zone (Swarup *et al.* 2007), this implies that the fibre angle will in general not remain

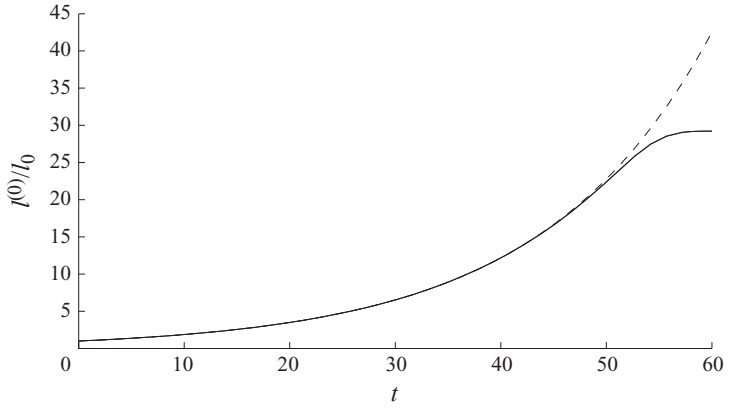

FIGURE 3. The length of the cell (rescaled with initial length) when $\phi = 0$. Solutions of (3.13b) are shown for $P = 1$, $Q = 1/2$ for constant matrix viscosity (dashed line, $\mu_0 = 1$); and for an increasing matrix viscosity (solid line, $\mu_0(t) = (\exp((t/45)^8) - 1)/100 + 1$ for illustration).

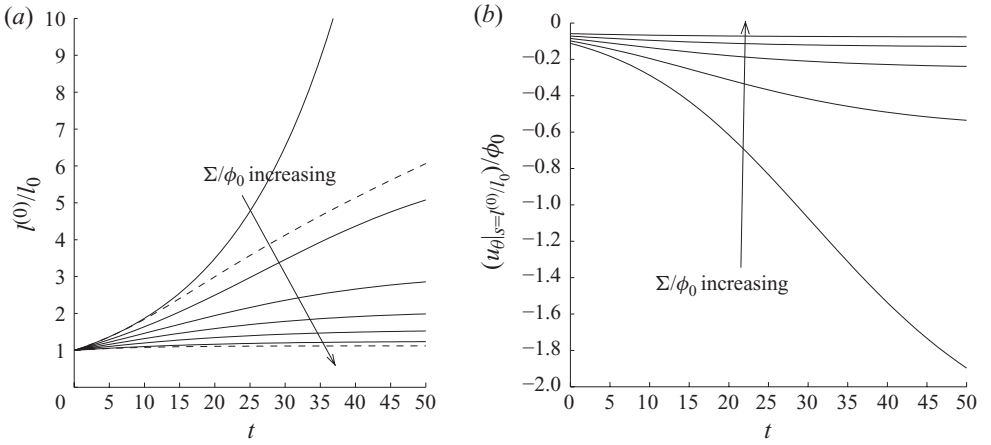

FIGURE 4. (a) The length of the cell (rescaled with initial length) and (b) the azimuthal velocity of the free end when $\phi_0 \ll 1$. Graphs are plotted with $Q = 1/2$, $\mu_3 = 1$ varying Σ/ϕ_0 between 0 and 0.1 in steps of 0.02, with $P = 1$ and $\mu_0 = 1$. In (a) the solutions of (3.30a) are plotted as solid lines; (b) shows solutions of (3.25b). The dashed lines in (a) show solutions of (D 14) for $\Sigma/\phi_0 = 0, 0.1$.

small and the expansion may ultimately become invalid. The zero-yield Lockhart-type cell-growth equation generalizes to (3.30a), which becomes

$$\frac{1}{l^*}\frac{\mathrm{d}l^*}{\mathrm{d}t^*} = \frac{1}{8\mu_0^* h_0}\left(R_0(P^* - Q^*) - \frac{4\phi_0 l^* \Sigma^*}{l_0^*}\right), \tag{4.3}$$

upon redimensionalization, differing from the horizontal fibre case only in the presence of an applied external torque, when additional nonlinearities appear. The axial growth rate of the cell depends on the cell geometry, the matrix viscosity and can ultimately be suppressed either by sufficient external torque (figure 4) or by stiffening of the matrix through $\mu_0^*(t^*)$. The fibre properties may interact with the torque but they primarily control the radial expansion, enforcing zero radius change at leading

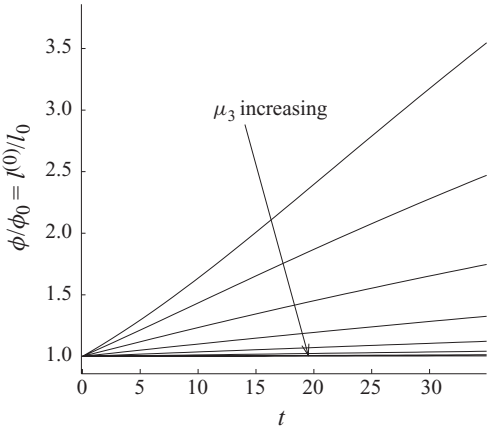

FIGURE 5. The length of the cell (rescaled with initial length) when $\phi_0 \ll 1$. The solution of (3.30*a*) is plotted, with $\Sigma = \mu_3\phi(P-Q)/4(\mu_0+\mu_3\phi^2)$ to enforce $u_\theta = 0$ (from (3.25*b*)). We take $Q = 1/2$, $P = 1$, $\mu_0 = 1$ and plot the solutions for $\mu_3 = 0.1$, 0.5, 1, 5, 10, 50, 100 and 500.

order and appearing within the expression for the small radius changes at next order (3.30*b*).

We plot the evolving normalized cell length (equivalent to the normalized fibre angle) and the azimuthal velocity of the end of the cell against time in figures 4 and 5, with constant internal pressure, matrix viscosity and external compressive force. The torque limits axial expansion of the cell and reorientation of the fibres (figure 4*a*); fibres with positive pitch induce rotation in the opposite sense (figure 4*b*) (see the $-M_3\tilde{\phi}^{(0)}$ term in (3.25*b*)) which is suppressed by torque aligned with the primary fibre direction. Provided the applied torque is small enough ($\Sigma^* \leqslant R_0^2(P^*-Q^*)/4\phi_0 l_0^*$), the length increases to a steady state such that

$$\frac{l^*}{l_0^*} = \frac{R_0\,(P^*-Q^*)}{\phi_0\,\Sigma^*}. \tag{4.4}$$

In contrast, if we apply a torque such that the azimuthal velocity is zero (see (3.25*b*)), the cell elongates indefinitely but grows more slowly if μ_3 (which contributes to the shear viscosity) is larger (figure 5). In this case μ_3 provides an additional mechanism for restraining cell expansion.

It is reasonably straightforward to extend the present approach to take into account variations in fibre orientation across the thickness of the wall, as happens when new fibres are deposited at a constant angle on the inner surface of the wall and are passively reorientated as they move towards the outer face of the wall by the elongational flow, as has been observed experimentally (Kutschera 2008; Anderson *et al.* 2010). For the small-angle case we derive a modified version of (3.30*a*) and (D 14) as shown in Appendix D, which becomes

$$\frac{1}{l^*}\frac{\mathrm{d}l^*}{\mathrm{d}t^*} = \frac{R_0\,(P^*-Q^*) - 4\phi_0(1+\log\left(l^*/l_0^*\right))\Sigma^*}{8h_0^*(\mu_0^*+\mu_3^*\phi_0^2(2l^*/l_0^* - 1 - (1+\log(l^*/l_0^*))^2))}, \tag{4.5}$$

upon redimensionalization. The effect of torque is reduced since fewer fibres are at the larger angle, reducing (but not eliminating) the capacity of passive fibre reorientation to suppress cell elongation, while μ_3 (which contributes to the shear viscosity) now appears even in the absence of torque and acts to reduce the expansion rate (figure 4*a*).

Finally, we consider the case in which the cell wall is inextensible in the fibre direction, the fibre angle need not be small and an external torque is applied to enforce zero radius change. A modified zero-yield Lockhart-type cell-growth equation (3.41) is found along with (3.39) for the fibre angle, which become

$$\frac{1}{l^*}\frac{\mathrm{d}l^*}{\mathrm{d}t^*} = \frac{R_0}{4h_0}\left(\frac{(1-3l^{*2}/l_0^{*2})P^* - (1-l^{*2}/l_0^{*2})Q^*}{\mu_0^*(2-3l^{*2}/l_0^{*2}) + \mu_3^* l^{*2}/l_o^{*2}}\right), \tag{4.6a}$$

$$\frac{\mathrm{d}\phi}{\mathrm{d}t^*} = \frac{R_0 \sin\phi}{4h_0\cos\phi}\left(\frac{(3\cos^2\phi - 2)P^* - \cos^2\phi\, Q^*}{\mu_0^*(3\cos^2\phi - 1) + \mu_3^* \sin^2\phi}\right), \tag{4.6b}$$

upon redimensionalization. Again, the axial growth is controlled by μ_3, as well as the matrix viscosity and the geometry of the cell. Assuming the fibre angle is relatively small initially, and the viscosities remain constant, the length will increase to the constant value given by (3.42), whereupon the fibres lock the cell length in place with tension in the fibres balancing the competing internal and external normal stresses P and Q as well as the external torque. This final length is determined by the geometry of the cell and the fibres only; there is no dependence on the material properties. We plot the cell length and fibre angle in figure 6 for fixed P and Q and varying ϕ_0 and μ_3. In all cases a steady state is achieved; the initial fibre angle controls the final cell length, while the same steady state is found for the cell length for varying μ_3 and the fibre angle in both cases. Increasing μ_3 slows the evolution to the steady state, while the cell may even shrink if ϕ_0 is sufficiently large.

5. Discussion

We have modelled the anisotropic expansion of a diffusely growing plant cell within the primary root elongation zone, describing the cell as a pressurized axisymmetric viscous sheet between rigid end plates. In doing so we have developed an extended framework for modelling extensional flows of thin sheets of fibre-reinforced materials.

In the simplified cases considered here, we have identified three mechanisms by which cell expansion is regulated. When the CMF are all orthogonal to the axis of the cell, the parameter μ_0 (representing the isotropic component of the matrix viscosity) is the primary determinant of the rate of cell elongation (assuming fixed turgor pressure and fixed external forcing). It is necessary for μ_0 to increase rapidly in time for the cell to stop its expansion, as illustrated in figure 3. The present model does not discriminate explicitly between the viscosity of the pectin matrix (modified by the presence of the fibres) and the properties of cross-links between fibres, both of which are under independent hormonal regulation in the expansion zone of the root. The primary role of the fibres in this case is to inhibit radial expansion as the cell elongates. If, instead, the fibres are tilted to have a small component in the cell-axis direction, then an external torque can contribute to saturation of the growth of the cell (figure 4*a*), as can the viscous parameter μ_3 associated with the anisotropic shear response of the fibrous material (which again is likely to be influenced indirectly by cross-linking molecules). When the fibre angle varies across the cell wall and new fibres are deposited at a constant angle, the growth rate exhibits a length-dependent slowing, even in the absence of an external torque (figure 4*a*). If the external torque inhibits rotation of the cell wall, despite the presence of tilted fibres (a plausible situation in a multicellular structure in which cells are tightly bonded to their neighbours), both μ_0 and μ_3 again determine the expansion rate (figure 5); the torque in this case can be considered as a residual moment. If the fibres are bonded to the matrix (and to each

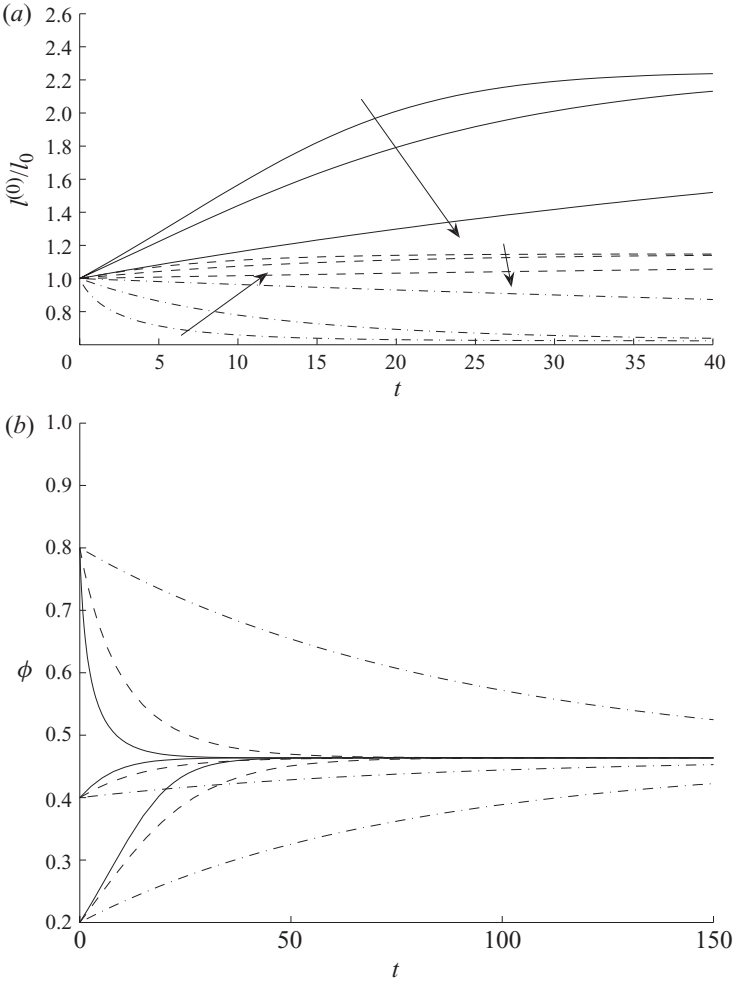

FIGURE 6. (*a*) The length of the cell (rescaled with initial length) and (*b*) fibre angle when the material is inextensible in the fibre direction. We take $Q = 1/2$, with $P = 1$ and $\mu_0 = 1$ without loss of generality, and vary both ϕ_0 and μ_3. In (*a*) the solution of (3.41) is shown with solid lines for $\phi_0 = 0.2$, dashed lines for $\phi_0 = 0.4$, dot-dash lines for $\phi_0 = 0.8$, and μ_3 is 1, 10 or 100 (arrows indicate increasing μ_3). In (*b*) the solution of (3.39) is shown with solid lines for $\mu_3 = 1$, dashed lines for $\mu_3 = 10$ and dot-dash lines for $\mu_3 = 100$, and ϕ_0 is 0.2, 0.4 or 0.8. In all cases the tension, T, is positive, and thus there is no risk of buckling.

other) sufficiently strongly to inhibit extension in the fibre direction, we showed that passive fibre reorientation (coupled to an external torque) can inhibit growth of the whole cell (figure 6). The final cell length is determined by the geometry of the system, with wall mechanical properties controlling the time taken to reach steady state. This conclusion has been postulated earlier (Carpita & Gibeaut 1993), lending credibility to this idea. In each of these cases, based on clearly identified sets of assumptions (which are undoubtedly an oversimplification of biological reality), we derived three analogues of well-known Lockhart-type cell-growth equation (1.2) that are rationally derived from a more fundamental constitutive law, giving insight into the effect of the evolving microstructure on the macroscopic cell properties.

Natural further refinements of the present model are to include the effects of yield stress in the constitutive law and to consider the effect of bending and torsion of the cell centreline. The model can also be readily scaled up to describe the behaviour of multiple non-axisymmetric cells, to yield expressions for the Lockhart cell-growth equation for a complete root, as we will report elsewhere.

The Centre for Plant Integrative Biology is a Centre for Integrative Systems Biology supported by BBSRC and EPSRC. We would like to thank all CPIB staff, in particular Darren Wells, for helpful discussions. O.E.J. acknowledges support from the Leverhulme Trust.

Appendix A. Geometry

Within this appendix we recall the relationship between the velocity of the centre-surface and the evolving geometry of the axisymmetric sheet, following VHO.

We denote the centre-surface of the sheet as $\boldsymbol{r}_c^*(s^*, \theta, t^*)$, such that

$$\boldsymbol{r}_c^* = R^* \cos\theta \boldsymbol{i} + R^* \sin\theta \boldsymbol{j} + z^* \boldsymbol{k}, \tag{A 1}$$

where $R^*(s^*, \theta, t^*)$ is the radius of the centre-surface, $z^*(s^*, t^*)$ is the vertical distance along the axis of the sheet, s^* is the body-fitted arclength (such that $\mathrm{d}s^{*2} = \mathrm{d}R^{*2} + \mathrm{d}z^{*2}$), θ is the polar angle, t^* is time and $\boldsymbol{i}, \boldsymbol{j}, \boldsymbol{k}$ are Cartesian base vectors. We may therefore define the (inward-pointing) unit normal to this surface to be

$$\boldsymbol{e}_n = \left| \frac{\partial \boldsymbol{r}_c^*}{\partial s^*} \wedge \frac{\partial \boldsymbol{r}_c^*}{\partial \theta} \right|^{-1} \left(\frac{\partial \boldsymbol{r}_c^*}{\partial s^*} \wedge \frac{\partial \boldsymbol{r}_c^*}{\partial \theta} \right), \tag{A 2}$$

and so represent any point within the fluid sheet by

$$\boldsymbol{r}^* = \boldsymbol{r}_c^* + n^* \boldsymbol{e}_n, \tag{A 3}$$

where the free surfaces are given by $n^* = \pm h^*(s^*, \theta, t^*)/2$. An orthonormal basis is given by $(\boldsymbol{e}_s, \boldsymbol{e}_\theta, \boldsymbol{e}_n)$ where

$$\boldsymbol{e}_s = \frac{\partial \boldsymbol{r}_c^*}{\partial s^*}, \qquad \boldsymbol{e}_\theta = \frac{1}{R^*} \frac{\partial \boldsymbol{r}_c^*}{\partial \theta}, \tag{A 4}$$

leading to the requirement

$$\frac{\partial \boldsymbol{r}_c^*}{\partial s^*} \cdot \frac{\partial \boldsymbol{r}_c^*}{\partial \theta} = 0. \tag{A 5}$$

The principal curvatures, κ_i^*, are defined via

$$\frac{\partial \boldsymbol{e}_n}{\partial s^*} = -\kappa_s^* \boldsymbol{e}_s, \qquad \frac{\partial \boldsymbol{e}_n}{\partial \theta} = -R^* \kappa_\theta^* \boldsymbol{e}_\theta, \tag{A 6}$$

and given by (2.6) and (2.7). Differentiating the base vectors (A 4) with respect to s^* and θ, and using (A 6) we find the usual identities linking R^*, κ_s^*, κ_θ^*; that is

$$\frac{\partial \kappa_s^*}{\partial \theta} = 0, \tag{A 7a}$$

$$R^* \frac{\partial \kappa_\theta^*}{\partial s} = \left(\kappa_s^* - \kappa_\theta^*\right) \frac{\partial R^*}{\partial s^*}, \tag{A 7b}$$

$$\frac{\partial^2 R^*}{\partial s^{*2}} + R^* \kappa_s^* \kappa_\theta^* = 0. \tag{A 7c}$$

We denote the velocity of the centre-surface by $\boldsymbol{v}^*$ such that

$$\frac{\partial \boldsymbol{r}_c^*}{\partial t^*} = v_s^* \boldsymbol{e}_s + v_\theta^* \boldsymbol{e}_\theta + v_n^* \boldsymbol{e}_n. \tag{A 8}$$

By differentiating (A 8) with respect to s^* and θ, (A 5) with respect to t^*, and using (A 4) along with that $\boldsymbol{e}_i$ are unit vectors, we find expressions (2.5) respectively for $\boldsymbol{v}^*$.

Appendix B. Derivation of thin sheet equations

In this appendix we detail how the system of equations is derived for the relevant small-aspect-ratio limit. As in Appendix A, this work closely follows that given in VHO but we record it here to keep this paper relatively self-contained.

B.1. *Expansion of strain-rate components*

We need to perform a regular expansion of the strain-rate components in terms of the small aspect ratio in order to determine stress tensor (2.4) for the simplified system. These strain-rate components are given (non-dimensionally) by (Aris 1962)

$$e_{ss} = \frac{1}{l_s}\left(\frac{\partial U_s}{\partial s} + \frac{U_\theta}{l_\theta}\frac{\partial l_s}{\partial \theta} + \frac{U_n}{\epsilon}\frac{\partial l_s}{\partial n}\right), \tag{B 1a}$$

$$e_{s\theta} = \frac{1}{2 l_s l_\theta}\left(l_s \frac{\partial U_s}{\partial \theta} - \frac{\partial l_s}{\partial \theta} U_s + l_\theta \frac{\partial U_\theta}{\partial s} - \frac{\partial l_\theta}{\partial s} U_\theta\right), \tag{B 1b}$$

$$e_{\theta\theta} = \frac{1}{l_\theta}\left(\frac{\partial U_\theta}{\partial \theta} + \frac{U_s}{l_s}\frac{\partial l_\theta}{\partial s} + \frac{U_n}{\epsilon}\frac{\partial l_\theta}{\partial n}\right), \tag{B 1c}$$

where l_i are the scaling factors for the metric $l_s^2\,\mathrm{d}s^2 + l_\theta^2\,\mathrm{d}\theta^2 + \epsilon^2 l_n^2\,\mathrm{d}n^2$ given by

$$l_s = 1 - \epsilon\kappa_s n, \quad l_\theta = R\,(1 - \epsilon\kappa_\theta n), \quad l_n = 1. \tag{B 2}$$

Expanding (B 1*a, b*) in powers of ϵ, using $u_n = 0$, substituting for $\kappa_i v_n$ from (2.9*a*) and (2.9*b*) and neglecting θ derivatives we find the components of the rate-of-strain tensor given in (2.17). Note that there is an additional term in the $e_{s\theta}$ component which is missing in VHO (see Howell 1998).

B.2. *Expansion of the evolution equation for the fibre director field*

We now consider the evolution equation for fibre director field (2.2), which in dimensionless variables is

$$\frac{\partial \boldsymbol{a}}{\partial t} + (\boldsymbol{U}\cdot\nabla)\,\boldsymbol{a} + \zeta \boldsymbol{a} = (\boldsymbol{a}\cdot\nabla)\,\boldsymbol{U}. \tag{B 3}$$

We again need to expand this in powers of the small aspect ratio ϵ, and write in terms of the velocity $\boldsymbol{u}$ relative to the moving centre-surface. Using index notation such that $s = x_1$, $\theta = x_2$ and $\epsilon n = x_3$, we can write (B 3) in component form (using the Einstein summation convention on j, k but not i), as (Aris 1962)

$$\frac{\partial a_i}{\partial t} + \frac{l_i}{l_j} U_j \frac{\partial}{\partial x_j}\left(\frac{a_i}{l_i}\right) + \frac{l_i}{l_j l_k}\Gamma^i_{jk} U_j a_k + \zeta a_i = \frac{l_i}{l_j} a_j \frac{\partial}{\partial x_j}\left(\frac{U_i}{l_i}\right) + \frac{l_i}{l_j l_k}\Gamma^i_{jk} a_j U_k, \tag{B 4}$$

where Γ^i_{jk} are the Christoffel symbols.

As j and k are dummy variables and the Christoffel symbols are symmetric in j and k, the Christoffel symbol terms cancel and we are left with

$$\frac{\partial a_i}{\partial t} + \frac{l_i}{l_j} U_j \frac{\partial}{\partial x_j}\left(\frac{a_i}{l_i}\right) + \zeta a_i = \frac{l_i}{l_j} a_j \frac{\partial}{\partial x_j}\left(\frac{U_i}{l_i}\right). \tag{B 5}$$

Expanding in powers of ϵ, using $u_n = 0$, substituting for $\kappa_i v_n$ from (2.9a) and (2.9b) and again neglecting θ-dependence, we find

$$\frac{\partial a_s}{\partial t} + U_s \frac{\partial a_s}{\partial s} - a_s \frac{\partial v_s}{\partial s} + \zeta a_s = a_s \frac{\partial U_s}{\partial s}, \tag{B 6a}$$

$$\frac{\partial a_\theta}{\partial t} + RU_s \frac{\partial}{\partial s}\left(\frac{a_\theta}{R}\right) - \frac{a_\theta}{R}\left(\frac{\partial R}{\partial t} - v_s \frac{\partial R}{\partial s}\right) + \zeta a_\theta = Ra_s \frac{\partial}{\partial s}\left(\frac{U_\theta}{R}\right). \tag{B 6b}$$

Now, using (2.9c) and defining $u_s = U_s - v_s$, $u_\theta = U_\theta - v_\theta$, we see that we have

$$\frac{\partial a_s}{\partial t} + (u_s + v_s)\frac{\partial a_s}{\partial s} + \zeta a_s = a_s \frac{\partial u_s}{\partial s}, \tag{B 7a}$$

$$\frac{\partial a_\theta}{\partial t} + (u_s + v_s)\frac{\partial a_\theta}{\partial s} + \zeta a_\theta = a_s \left(\frac{\partial u_\theta}{\partial s} - \frac{u_\theta}{R}\frac{\partial R}{\partial s}\right) + \frac{a_\theta}{R}\frac{\mathrm{D}R}{\mathrm{D}t}. \tag{B 7b}$$

Finally, since $a_s = \sin\phi$, $a_\theta = \cos\phi$, upon taking suitable linear combinations of (B 7a) and (B 7b) we find the evolution equation for director field angle (2.13), and the relative length change of a section of fibre (2.14).

B.3. *Expansion of the evolution equation for the fibre density*

We now consider the evolution equation for fibre density (2.3), and perform a similar expansion to (B.2). We can write (2.3) in non-dimensional form as

$$\frac{\partial \rho}{\partial t} + \frac{1}{l_1 l_2}\frac{\partial}{\partial x_j}\left(\frac{l_1 l_2}{l_j}\rho U_j\right) = G(\boldsymbol{x}, t), \tag{B 8}$$

using summation notation (Aris 1962). Upon expansion in terms of small ϵ, using $u_n = 0$, substituting for $\kappa_i v_n$ from (2.9a) and (2.9b) and again neglecting θ dependence, we find

$$\frac{\partial \rho}{\partial t} + (u_s + v_s)\frac{\partial \rho}{\partial s} + \rho\left(\frac{1}{R}\frac{\mathrm{D}R}{\mathrm{D}t} + \frac{\partial u_s}{\partial s}\right) = G(s, t), \tag{B 9}$$

where $u_s = U_s - v_s$.

Appendix C. Consistency of asymptotic limits

Within § 3.2 we examined the governing equations in the small-fibre-angle limit, with μ_2 large (but not infinite) to suppress radius changes at leading order. In § 3.3 we allowed general fibre angle but took the fibres to be completely inextensible, so that $\mu_2 \to \infty$, $\zeta \to 0$ where $\mu_2 \zeta = \hat{T}$ is of order one. In this case we applied an appropriate torque to the growing end of the cell to suppress radius changes.

We take $M_2 \to \infty$ in § 3.2, reducing (3.27) to

$$\frac{\mathrm{D}^{(0)} R^{(1)}}{\mathrm{D}t} = \frac{(P - Q)\tilde{\phi}^{(0)2}}{8\mu_0} - \frac{\left(2\mu_0 + M_3 \tilde{\phi}^{(0)2}\right)\tilde{\phi}^{(0)}\tilde{\Sigma}}{2\mu_0 M_3}. \tag{C 1}$$

Thus, applying a torque of the form

$$\tilde{\Sigma} = \frac{(P - Q)\tilde{\phi}^{(0)} M_3}{4\left(2\mu_0 + M_3 \tilde{\phi}^{(0)2}\right)}, \tag{C 2}$$

suppresses the next-order radius changes; applying this torque within § 3.2 should give a similar solution to that found in § 3.3. The velocity components become

(from (3.25))

$$u_s^{(0)} = \frac{P-Q}{4\left(2\mu_0 + M_3\tilde{\phi}^{(0)^2}\right)}s, \quad \tilde{u}_\theta^{(0)} = \frac{P-Q}{4\left(2\mu_0 + M_3\tilde{\phi}^{(0)^2}\right)}\tilde{\phi}^{(0)}s, \tag{C 3}$$

along with (from (3.24), (C 3*a*))

$$\frac{1}{\tilde{\phi}^{(0)}}\frac{\mathrm{d}\tilde{\phi}^{(0)}}{\mathrm{d}t} = \frac{P-Q}{4\left(2\mu_0 + M_3\tilde{\phi}^{(0)^2}\right)}, \tag{C 4}$$

for the fibre angle such that $\tilde{\phi}^{(0)} = l^{(0)}$.

Scaling $\phi = \delta\tilde{\phi}$, $\Sigma = \tilde{\Sigma}/\delta$, $u_\theta = \delta\tilde{u}_\theta$ with $\mu_3\delta^2 = M_3$ in § 3.3, the applied torque (3.36) becomes (C 2), velocity components (3.33) with (3.38*d*) become (C 3) and finally the ODE for fibre angle (3.39) becomes (C 4) with the length of cell (3.40) reducing to (3.29).

Appendix D. Distribution of fibre angle across the wall

In this appendix we consider variations in fibre angle across the cell wall. During growth, fibres are continually laid down on the inner face of the wall and are passively reorientated (according to evidence from Anderson *et al.* 2010). We assume here that fibres are deposited at a fixed, small angle ϕ_0 on the inner wall, but that the fibre angle increases as the fibres are carried through the elongating wall. We assume the wall has uniform thickness $h = 1$.

We first reconsider the integration of the stress tensor with respect to n between $-1/2$ and $1/2$ (given by (2.18)) since variations in fibre angle across the wall lead to a dependence on n within (2.4). If we replace ha_s^2, ha_sa_θ, ha_θ^2, $ha_s^2\zeta$, $ha_sa_\theta\zeta$ and $ha_\theta^2\zeta$ with barred quantities such that

$$\overline{a_s^2} = \int_{-1/2}^{1/2} a_s^2 \,\mathrm{d}n, \tag{D 1}$$

the analysis will follow through as described in this paper. (While fibre orientations may vary rapidly with n, we expect the velocity field in the wall to remain slowly varying with n.) By calculating the fibre angle variation through the wall, we can therefore easily modify the model to take this effect into account.

For illustrative purposes we consider the small-fibre-angle case as described in § 3.2, again assuming the cell is cylindrical with $R^{(0)} = 1$. Assuming $u_s = As$ in $0 < s < l(t)$, where $A = (1/l)\,\mathrm{d}l/\mathrm{d}t$ and so $l = l_0\mathrm{e}^{At}$, the leading-order components of (3.22*b, c*) may be written as

$$\frac{P-Q}{2} = 4\mu_0 A + 4\mu_3\left(\frac{1}{2}\overline{a_sa_\theta}\frac{\partial u_\theta}{\partial s} + \overline{a_s^2}A\right), \tag{D 2}$$

$$\Sigma = 2\mu_3\left(\frac{1}{2}\frac{\partial u_\theta}{\partial s} + \overline{a_sa_\theta}A\right), \tag{D 3}$$

and hence

$$\frac{P-Q}{2} = 4\mu_0 A + 4\mu_3\overline{a_s^2}A + 2\overline{a_sa_\theta}\left(\Sigma - 2\mu_3\overline{a_sa_\theta}A\right). \tag{D 4}$$

We now determine the fibre kinematics, assuming stretching commences at $t = 0$. Conservation of mass in the wall gives

$$\frac{\partial u_s}{\partial s} + \frac{\partial u_n}{\partial n} = 0. \tag{D 5}$$

Taking $u_n = 0$ on $n = 1/2$, we find

$$u_n = A\left(\tfrac{1}{2} - n\right). \tag{D 6}$$

Thus $u_n = A$ on the inner wall at $n = -1/2$, representing deposition of new material as in (2.1a). A fibre deposited onto the inner face of the wall at time $t = t_0 \geqslant 0$ moves into the wall on the cylindrical surface satisfying

$$\frac{\mathrm{d}n}{\mathrm{d}t} = A\left(\frac{1}{2} - n\right), \tag{D 7}$$

giving

$$n = \tfrac{1}{2}\left(1 - 2\mathrm{e}^{-A(t-t_0)}\right). \tag{D 8}$$

Along this path, ϕ evolves according to (2.13) with $R = R^{(0)}$ and $v_s = 0$. Taking the small angle limit ($\phi \ll 1$) as in § 3.2 this reduces to

$$\frac{\partial \phi}{\partial t} + As\frac{\partial \phi}{\partial s} = A\phi, \tag{D 9}$$

and hence $\mathrm{d}\phi/\mathrm{d}t = A\phi$ on characteristics (D 7) and $\mathrm{d}s/\mathrm{d}t = As$, giving $\phi = \phi_0 \mathrm{e}^{A(t-t_0)}$ on (D 8). Thus the distribution of fibres deposited since the initiation of stretching satisfies

$$\phi = \frac{2\phi_0}{1 - 2n} \tag{D 10}$$

for $-1/2 \leqslant n \leqslant N = (1 - 2\mathrm{e}^{-At})/2 = 1/2 - l_0/l$.

We assume that initially the fibres throughout the wall are at a uniform angle ϕ_0. These fibres will then evolve during the motion according to (3.29), i.e.

$$\phi = \phi_0 / \left(\tfrac{1}{2} - N\right), \tag{D 11}$$

and lie in the shrinking domain $N \leqslant n \leqslant 1/2$.

We therefore find, from (D 1), (D 10) and (D 11), that

$$\overline{a_s a_\theta} = \phi_0\left(1 + \log\left(l/l_0\right)\right), \tag{D 12}$$

$$\overline{a_s^2} = \phi_0^2\left(2l/l_0 - 1\right), \tag{D 13}$$

and so

$$\frac{1}{l}\frac{\mathrm{d}l}{\mathrm{d}t} = \frac{P - Q - 4\phi_0\left(1 + \log\left(l/l_0\right)\right)\Sigma}{8(\mu_0 + \mu_3\phi_0^2(2l/l_0 - 1 - (1 + \log(l/l_0))^2))}, \tag{D 14}$$

in contrast to (3.30a) for constant fibre angle throughout the wall.

REFERENCES

Anderson, C. T., Carroll, A., Akhmetova, L. & Somerville, C. 2010 Real time imaging of cellulose reorientation during cell wall expansion in arabidopsis roots. *Plant Physiol.* **152**, 787–796.

Aris, R. 1962 *Vectors, Tensors and the Basic Equations of Fluid Mechanics*. Prentice-Hall (reprinted 1989 Dover).

Baskin, T. I. 2001 On the alignment of cellulose microfibrils by cortical microtubules: A review and a model. *Protoplasma* **215**, 150–171.

Baskin, T. I. 2005 Anisotropic expansion of the plant cell wall. *Annu. Rev. Cell Dev. Biol.* **21**, 203–222.

Batchelor, G. K. 1970 The stress system in a suspension of force-free particles. *J. Fluid Mech.* **41** (3), 545–570.

Batchelor, G. K. 1971 The stress generated in a non-dilute suspension of elongated particles by pure straining motion. *J. Fluid Mech.* **46**, 813–829.

Ben Amar, M. & Cummings, L. J. 2001 Fingering instabilities in driven thin nematic films. *Phys. Fluids* **13** (5), 1160–1166.

Bruce, D. M. 2003 Mathematical modelling of the cellular mechanics of plants. *Phil. Trans. R. Soc. Lond.* B **358**, 1437–1444.

Carpita, N. C. & Gibeaut, D. M. 1993 Structural models of primary-cell walls in flowering plants – consistency of molecular-structure with the physical-properties of the walls during growth. *Plant J.* **3** (1), 1–30.

Chaplain, M. A. J. 1993 The strain-energy function of an ideal plant-cell wall. *J. Theor. Biol.* **163** (1), 77–97.

Chavarria-Krauser, A., Jager, W. & Schurr, U. 2005 Primary root growth: A biophysical model of auxin-related control. *Func. Plant Biol.* **32** (9), 849–862.

Cosgrove, D. J. 2005 Growth of the plant cell wall. *Nat. Rev. Mol. Cell Bio.* **6** (11), 850–861.

Cowdrey, D. R. & Preston, R. D. 1966 Elasticity and microfibrillar angle in wood of sitka spruce. *Proc. R. Soc. B-Biol. Sci.* **166** (1004), 245–272.

Davies, G. C., Hiller, S. & Bruce, D. M. 1998 A membrane model for elastic deflection of individual plant cell walls. *J. Texture Stud.* **29** (6), 645–667.

Derbyshire, P., Findlay, K., McCann, M. C. & Roberts, K. 2007*a* Cell elongation in Arabidopsis hypocotyls involves dynamic changes in cell wall thickness. *J. Exp. Bot.* **58** (8), 2079–2089.

Derbyshire, P., McCann, M. C. & Roberts, K. 2007*b* Restricted cell elongation in Arabidopsis hypocotyls is associated with a reduced average pectin esterification level. *BMC Plant Biol.* **7**, 31–43.

Dolan, L. & Davies, J. 2004 Cell expansion in root. *Curr. Opin. Cell Biol.* **7**, 33–39.

Dumais, J., Shaw, S. L., Steele, C. R., Long, S. R. & Ray, P. M. 2006 An anisotropic–viscoplastic model of plant cell morphogenesis by tip growth. *Intl J. Dev. Biol.* **50**, 209–222.

Ericksen, J. L. 1960 Transversely isotropic fluids. *Colloid Polym. Sci.* **173** (2), 117–122.

van de Fliert, B. W., Howell, P. D. & Ockendon, J. R. 1995 Pressure-driven flow of a thin viscous sheet. *J. Fluid Mech.* **292**, 359–376.

Geitmann, A. 2006 Plant and fungal cytomechanics: quantifying and model cellular architecture. *Can. J. Bot.* **84**, 581–593.

Gertel, E. T. & Green, P. B. 1977 Cell growth pattern and wall microfibrillar arrangement: Experiments with nitella. *Plant Physiol.* **60** (2), 247–254.

Goriely, A., Robertson-Tessi, M., Tabor, M. & Vandiver, R. 2008 Elastic growth models. In *Mathematical Modelling of Biosystems*, pp. 1–44. Springer.

Green, P. B. 1960 Multinet growth in the cell wall of Nitella. *J. Cell Biol.* **7** (2), 289–296.

Green, P. B. 1968 Growth physics in Nitella: A method for continuous in vivo analysis of extensibility based on a micro-manometer technique for turgor pressure. *Plant Physiol.* **43** (8), 1169–1184.

Green, J. E. F. & Friedman, A. 2008 The extensional flow of a thin sheet of incompressible, transversely isotropic fluid. *Euro. J. Appl. Math.* **19** (3), 225–257.

Hamant, O., Heisler, M. G., Jonsson, H., Krupinski, P., Uyttewaal, M., Bokov, P., Corson, F., Sahlin, P., Boudaoud, A., Meyerowitz, E. M., Couder, Y. & Traas, J. 2008 Developmental patterning by mechanical signals in arabidopsis. *Science* **322** (5908), 1650–1655.

Hand, G. L. 1962 A theory of anisotropic fluids. *J. Fluid Mech* **13** (1), 33–46.

Hettiaratchi, D. R. P. & O'Callaghan, J. R. 1978 Structural mechanics of plant-cells. *J. Theor. Biol.* **74** (2), 235–257.

Holzapfel, G. A., Gasser, T. C. & Ogden, R. W. 2000 A new constitutive framework for arterial wall mechanics and a comparative study of material models. *J. Elasticity* **61** (1–3), 1–48.

Howell, P. D. 1998 Models for thin viscous sheets (vol 7, 32, 1996). *Euro. J. Appl. Math.* **9** (1), 93.

Jarvis, M. C. 1984 Structure and properties of pectin gels in plant-cell walls. *Plant Cell Environ.* **7** (3), 153–164.

Jeffery, G. B. 1922 The motion of ellipsoidal particles immersed in a viscous fluid. *Proc. Roy. Soc.* A **102** (715), 161–179.

Kerstens, S. & Verbelen, J. P. 2003 Cellulose orientation at the surface of the Arabidopsis seedling. Implications for the biomechanics in plant development. *J. Struct. Biol.* **144** (3), 262–270.

Kutschera, U. 2008 The growing outer epidermal wall: Design and physiological role of a composite structure. *Ann. Bot.-Lond.* **101** (5), 615–621.

Lee, M. E. M. & Ockendon, H. 2005 A continuum model for entangled fibres. *Euro. J. Appl. Math.* **16**, 145–160.

Lindenmayer, A., Prusinkiewicz, P., Hanan, J. S., Fracchia, F. D., Fowler, D. R., de Boer, M. J. M. & Mercer, L. 1996 *The Algorithmic Beauty of Plants*. Springer-Verlag.

Lipscomb, G. G., Denn, M. M., Hur, D. U. & Boger, D. V. 1988 The flow of fibre suspensions in complex geometries. *J. Non-Newton. Fluid Mech.* **26** (3), 297–325.

Lloyd, C. & Chan, J. 2004 Microtubules and the shape of plants to come. *Nat. Rev. Mol. Cell Bio.* **5** (1), 13–22.

Lockhart, J. A. 1965 An analysis of irreversible plant cell elongation. *J. Theor. Biol.* **8**, 264–275.

Marga, F., Grandbois, M., Cosgrove, D. J. & Baskin, T. I. 2005 Cell wall extension results in the coordinate separation of parallel microfibrils: Evidence from scanning electron microscopy and atomic force microscopy. *Plant J.* **43** (2), 181–190.

McQueen-Mason, S. J. & Cosgrove, D. J. 1995 Expansin mode of action on cell-walls – Analysis of wall hydrolysis, stress-relaxation, and binding. *Plant Physiol.* **107** (1), 87–100.

Ortega, J. K. E. 1985 Augmented growth equation for cell-wall expansion. *Plant Physiol.* **79** (1), 318–320.

Passioura, J. B. & Fry, S. C. 1992 Turgor and cell expansion – Beyond the Lockhart equation. *Aust. J. Plant. Physiol.* **19** (5), 565–576.

Pitt, R. E. & Davis, D. C. 1984 Finite-element analysis of fluid-filled cell response to external loading. *Trans. ASAE* **27** (6), 1976–1983.

Probine, M. C. 1963 Cell growth and the structure and mechanical properties of the wall in internodal cells of Nitella opaca. III. Spiral growth and cell wall structure. *J. Exp. Bot.* **14** (1), 101–113.

Probine, M. C. & Preston, R. D. 1961 Cell growth and the structure and mechanical properties of the wall in internodal cells of Nitella opaca. I. Wall structure and growth. *J. Exp. Bot.* **12** (2), 261–282.

Probine, M. C. & Preston, R. D. 1962 Cell growth and the structure and mechanical properties of the wall in internodal cells of Nitella opaca. II. Mechanical properties of the walls. *J. Exp. Bot.* **13** (1), 111–127.

Proseus, T. E., Ortega, J. K. E. & Boyer, J. S. 1999 Separating growth from elastic deformation during cell enlargement. *Plant Physiol.* **119** (2), 775–784.

Proseus, T. E., Zhu, G. L. & Boyer, J. S. 2000 Turgor, temperature and the growth of plant cells: Using Chara corallina as a model system. *J. Exp. Bot.* **51** (350), 1481–1494.

Richmond, P. A., Metraux, J. P. & Taiz, L. 1980 Cell expansion patterns and directionality of wall mechanical-properties in Nitella. *Plant Physiol.* **65** (2), 211–217.

van Sandt, V. S. T., Suslov, D., Verbelen, J.-P. & Vissenberg, K. 2007 Xyloglucan endotransglucosylase activity loosens a plant cell wall. *Ann. Bot.-Lond.* **100**, 1467–1473.

Scheres, B., Benfey, P. & Dolan, L. 2002 Root development. In *The Arabiposis Book*. American Society of Plant Biologists.

Schopfer, P. 2006 Biomechanics of plant growth. *Am. J. Bot.* **93** (10), 1415–1425.

Sellen, D. B. 1983 The response of mechanically anisotropic cylindrical cells to multiaxial stress. *J. Exp. Bot.* **34** (143), 681–687.

Smith, L. G. & Oppenheimer, D. G. 2005 Spatial control of cell expansion by the plant cytoskeleton. *Annu. Rev. Cell Dev. Biol.* **21**, 271–295.

Somerville, C., Bauer, S., Brininstool, G., Facette, M., Hamann, T., Milne, J., Osborne, E., Paredez, A., Persson, S., Raab, T., Vorwerk, S. & Youngs, H. 2004 Toward a systems approach to understanding plant-cell walls. *Science* **306** (5705), 2206–2211.

Spencer, A. J. M. 1972 *Deformations of Fibre-Reinforced Materials*. Oxford University Press.

Suslov, D. & Verbelen, J.-P. 2006 Cellulose orientation determines mechanical anisotropy in onion epidermis cell walls. *J. Exp. Bot.* **57** (10), 2183–2192.

Swarup, R., Kramer, E. M., Perry, P., Knox, K., Leyser, H. M. O, Haseloff, J., Beemster, G. T. S, Bhalerao, R. & Bennett, M. J. 2005 Root gravitropism requires lateral root cap and epidermal cells for transport and response to a mobile auxin signal. *Nat. Cell Biol.* **7** (11), 1057–1065.

Swarup, R., Perry, P., Hagenbeek, D., der Straeten, D. Van, Beemster, G. T. S., Sandberg, G., Bhalerao, R., Ljung, K. & Bennett, M. J. 2007 Ethylene upregulates auxin biosynthesis in arabidopsis seedlings to enhance inhibition of root cell elongation. *The Plant Cell* **19** (7), 2186–2196.

Taiz, L. 1984 Plant cell expansion: Regulation of cell wall mechanical properties. *Ann. Rev. Plant. Physiol.* **35**, 585–657.

Taiz, L. & Zeiger, E. 2002 *Plant Physiology*, 3rd edn. Sinauer Associates.

Tanimoto, E., Fujii, S., Yamamoto, R. & Inanaga, S. 2000 Measurement of viscoelastic properties of root cell walls affected by low pH in lateral roots of Pisum sativum L. *Plant Soil* **226** (1), 21–28.

Thompson, D. S. 2001 Extensiometric determination of the rheological properties of the epidermis of growing tomato fruit. *J. Exp. Bot.* **52** (359), 1291–1301.

Thompson, D. S. 2005 How do cell walls regulate plant growth. *J. Exp. Bot.* **56** (419), 2275–2285.

Tomos, D. 2000 The plant cell pressure probe. *Biotech. Lett.* **22** (6), 437–442.

Trouton, F. T. 1906 On the coefficient of viscous traction and its relation to that of viscosity. *Proc. Roy. Soc.* **77A**, 426–440.

Veytsman, B. A. & Cosgrove, D. J. 1998 A model of cell wall expansion based on thermodynamics of polymer networks. *Biophys. J.* **75**, 2240–2250.

Zhu, G. L. & Steudle, E. 1991 Water transport across maize roots – simultaneous measurement of flows at the cell and root level by double pressure probe technique. *Plant Physiol.* **95** (1), 305–315.